https://doi.org/10.5194/egusphere-2025-5358
Preprint. Discussion started: 7 November 2025

Improving the precision of Antarctic GNSS time series through non-tidal loading corrections

Aino Schulz[1], Yohannes Getachew Ejigu[1], Jyri Näränen[2], Maaria Nordman[1,2]

[1]Department of Built Environment, School of Engineering, Aalto University, Espoo, 02150, Finland
[2]Finnish Geospatial Research Institute, National Land Survey of Finland, Espoo, 02150, Finland

Correspondence to: Aino Schulz (aino.schulz@aalto.fi)

Abstract. Precise Global Navigation Satellite System (GNSS) measurements are essential for monitoring vertical land motion in Antarctica, where geophysical processes such as glacial isostatic adjustment (GIA) and ice mass change produce complex and often subtle deformation signals. However, a substantial portion of the variability in GNSS time series is caused by non-tidal loading (NTL), which can bias trend estimates and obscure geophysical signals if left uncorrected. This study evaluates the impact of 11 NTL correction model combinations from EOST (École & Observatoire des Sciences de la Terre, Strasbourg) and ESMGFZ (Earth System Modelling Group of GeoForschungsZentrum Potsdam) on vertical GNSS time series at three East Antarctic stations located in Dronning Maud Land (DML) using five datasets processed with distinct strategies. Results show that NTL corrections substantially reduce root mean square (RMS), noise, and seasonal amplitudes in datasets with high initial variability, particularly in precise point positioning (PPP)-based solutions, while network-based and combined solutions show limited improvement or even increased variability. Among loading components, non-tidal atmospheric loading (NTAL) consistently yielded the greatest reductions, while the added contribution of non-tidal oceanic (NTOL) and hydrological (HYDL) loading were beneficial only in specific GFZ model combinations in PPP-processed datasets. GFZ corrections generally outperformed EOST at two stations, where RMS values were reduced by more than 20 %. On the other hand, EOST corrections were more effective at one station, where RMS values were reduced by approximately 15 %. These results demonstrate the critical role of processing strategy, NTL model choice, and station environment in improving Antarctic GNSS time series for geophysical interpretation.

1 Introduction

Precise geodetic measurements of vertical land motion are essential for studying a wide range of geophysical processes in climatically sensitive regions such as Antarctica. These processes include postglacial rebound and glacial isostatic adjustment (GIA), tectonic deformation, orogeny, sea-level rise, and transient phenomena such as earthquakes, volcanic activity, hydrological and cryospheric loading (Gobron et al., 2021; He et al., 2017; Hohensinn et al., 2024; Plag et al., 2010). In Antarctica, vertical land motion reflects both short-term variability and long-term signals associated with ice sheet mass change (Pan et al., 2025). Observations from the Global Navigation Satellite System (GNSS) capture signals related to mass

https://doi.org/10.5194/egusphere-2025-5358
Preprint. Discussion started: 7 November 2025

redistribution across the Earth system, including the solid Earth, oceans, atmosphere, cryosphere, and terrestrial water, and provide critical constraints for modelling these processes. Seasonal variations in estimated GNSS site positions are primarily driven by gravitational influences on atmospheric and water masses, thermally and hydrologically induced surface deformations, and residual systematic errors such as draconitic signals caused by satellite orbit mismodelling or errors in data processing (Altamimi et al., 2016; He et al., 2017).

A substantial portion of the seasonal and interannual variability observed in GNSS time series is caused by non-tidal loading (NTL), which includes non-tidal atmospheric (NTAL), oceanic (NTOL), and hydrological loading (HYDL). These surface mass redistributions induce elastic deformation of the Earth's crust, resulting in vertical displacements of up to several centimetres (Glomsda et al., 2023). NTL effects can account for up to 40 % of the seasonal signals observed in GNSS position time series (Dong et al., 2002; Van Dam and Wahr, 1998) and applying NTAL and NTOL corrections has been shown to reduce GNSS height variance by 20–30 % (Williams and Penna, 2011). Although some studies report variability across correction models and processing strategies (Jiang et al., 2013), global-scale NTL models generally exhibit small differences, often less than 2 %, in their impact on seasonal amplitudes and scatter (Mémin et al., 2020; Rebischung et al., 2024).

Applying NTL corrections is therefore not only beneficial for reducing variance and improving interpretation of geophysical signals but also critical for meeting the accuracy goals set by the Global Geodetic Observing System (GGOS), which targets 1 mm positional accuracy and 0.1 mm/yr velocity stability for terrestrial reference frames (Plag et al., 2010). Unmodelled loading effects can bias vertical velocity estimates by up to 1 mm/yr, exceeding these thresholds and compromising the ability to reliably monitor processes like sea level rise, ice mass loss, and other climate-related changes (Kotsakis and Chatzinikos, 2023). Furthermore, loading effects affect the accuracy of the International Terrestrial Reference Frame (ITRF) and Earth orientation parameters (EOP), which can introduce systematic errors in station coordinates, distort the realization of global reference frames, and degrade the precision of Earth rotation modelling (Glomsda et al., 2022; Mémin et al., 2020). Improving models of station coordinate trajectories by accounting for environmental loading can help construct more stable and consistent reference frames (Altamimi et al., 2016; Bevis et al., 2020).

There have been numerous regional (Ejigu et al., 2024; Ejigu and Nordman, 2025; Hohensinn et al., 2024; Khorrami et al., 2024; Klos et al., 2021; Martens et al., 2020; Nordman et al., 2015; Springer et al., 2019) and global (Dong et al., 2002; Gobron et al., 2021; Jiang et al., 2013; Männel et al., 2019; Mémin et al., 2020; Santamaría-Gómez and Mémin, 2015; Van Dam et al., 2012; Van Dam et al., 1994; Van Dam and Wahr, 1998) studies on the effects of NTL on GNSS time series. Research specifically focused on Antarctica remains limited (Andrei et al., 2018; Koulali et al., 2022; Buchta et al., 2025c; Liu et al., 2018; Pan et al., 2025), although several global analyses have incorporated data from Antarctic stations. Despite their importance, applying NTL corrections remains challenging particularly in polar regions due to model limitations, signal correlations, and inherent noise in GNSS data. GNSS station position time series contain both deterministic and stochastic signals, including seasonal components typically modelled with fixed annual and semi-annual terms, and non-deterministic components often estimated using Kalman filters (Gobron et al., 2024; He et al., 2017).

https://doi.org/10.5194/egusphere-2025-5358
Preprint. Discussion started: 7 November 2025

However, fully separating these signals is difficult because their stochastic properties are often correlated with coloured noise, which may itself contain valuable geophysical information. Stochastic variations in GNSS time series show both temporal and spatial correlations, with noise commonly represented as a combination of white noise (WN) and power-law (PL) components (Gobron et al., 2024). In polar regions, WN estimates are often extremely low, approaching zero, whereas PL noise can be very high, with amplitudes peaking around 10 mm/yr$^{1/4}$ before NTL corrections (Ejigu and Nordman, 2025; Gobron et al., 2021; Williams et al., 2004). Some of the spatially correlated noise has been attributed to reference frame errors and orbit modelling inaccuracies. Regional GNSS solutions often display lower noise levels, depending on network extent, inter-site distances, and the number and quality of stations available to estimate and mitigate common mode errors.

Given this context, this study aims to evaluate the impact of NTL corrections on GNSS time series in East Antarctica, focusing on three stations located in Dronning Maud Land (DML). While NTL corrections are widely applied in global studies, relatively few have examined their effectiveness in Antarctica, where unique geophysical conditions, limited spatial coverage of geodetic measurements, and elevated noise levels may alter correction performance. By comparing multiple correction models and GNSS datasets, this study contributes to a better understanding of the regional variability in NTL effects and the suitability of existing models in the Antarctic context. These insights are essential for improving accuracy of Antarctic GNSS time series, refining regional and global reference frames, and ensuring the reliable detection of long-term geophysical signals.

2 Data description

2.1 GNSS data and processing

This study focuses on three GNSS stations in DML, East-Antarctica: the Finnish ABOA, the Japanese SYOG, and the South-African VESL stations (Figure 1). These stations were selected due to their long and relatively continuous observations, each with more than 18 years of data, which represent some of the longest GNSS time series available on the continent. For a study of this type, it is prudent to concentrate on a limited number of stations in detail, both because of computational constraints and because of the limited number of stations with similarly long records. In addition, the three stations are geographically close in East-Antarctic terms but in distinct environmental settings: SYOG is located on an island, while ABOA and VESL are further inland, approximately 130 – 160 km from the ice shelf edge, which may affect the surface mass loading signals observed at each site. Unlike the more densely instrumented Antarctic Peninsula and Transantarctic Mountains, East Antarctica remains sparsely covered by geodetic infrastructure, with GNSS stations generally confined to exposed bedrock near the coast (Andrei et al., 2018; Buchta et al., 2025c). The availability of exposed bedrock is the main constraint on station placement, as stable monumentation is not possible on ice sheets or ice shelves due to their continuous flow. Ice motion is depth-dependent and varies across the ice sheet, influenced by ice thickness and basal topography (Reading et al., 2022; Sandells and Flocco, 2022), which would introduce non-tectonic movement to geodetic time series.

https://doi.org/10.5194/egusphere-2025-5358
Preprint. Discussion started: 7 November 2025

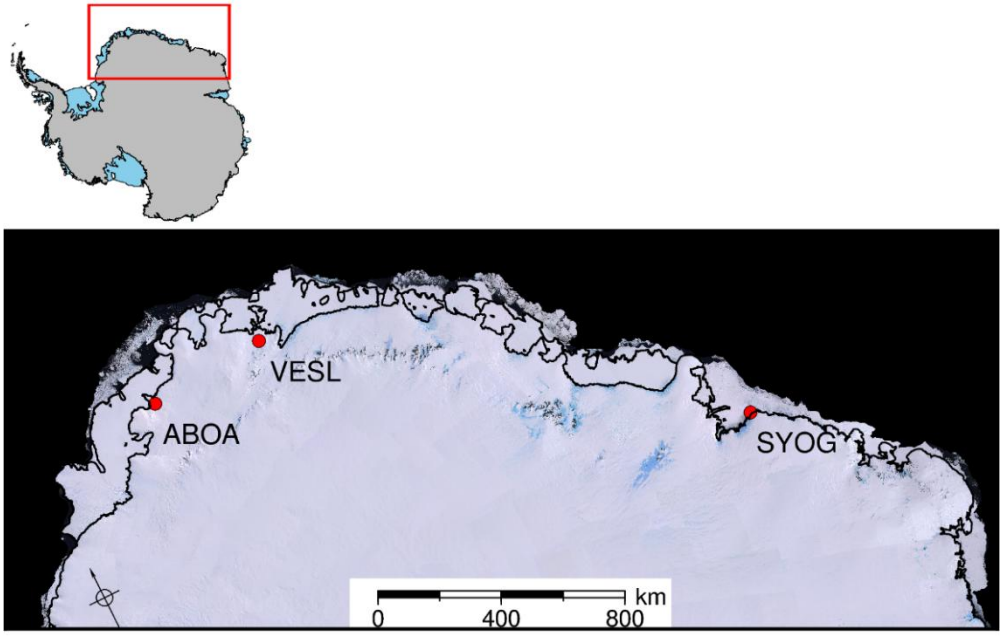

Figure 1: Location of the GNSS stations used in this study, marked with red points. The map was made with the Python library PolarToolkit (Tankersley, 2024).

This study compares five GNSS datasets derived from three processing sources: the Nevada Geodetic Laboratory (NGL) (Blewitt et al., 2018), the GIANT-REGAIN (GR, Geodynamics In ANTarctica based on REprocessing GNSS dAta Initiative) project (Buchta et al., 2025b), and an in-house solution referred to as AY (Aalto Yliopisto/University). The GR dataset is a combination solution, generated by merging four solutions from different analysis centres: Technical University of Dresden (TUD), University of Tasmania (UTAS), Ohio State University (OSU), and Newcastle University (NEWC). In addition to the combined GR dataset, two of its contributing solutions (TUD and OSU) were analysed separately to assess the impact of processing strategies and NTL corrections. These two solutions were selected as they represent the two extremes of the observed variation (Buchta et al., 2025c). Out of the five datasets, NGL does not include ABOA in their processing. A summary of the datasets and their processing characteristics is provided in Table 1.

Table 1: Summary of GNSS datasets used in this study and their processing characteristics.

Dataset	*Source*	*Strategy*	*Reference Frame*	*Software*	*Satellite System*	*NTL corrections*
AY	Aalto University	PPP	IGS20	GipsyX v2.3	GPS only	Not applied
NGL	Nevada Geodetic Laboratory	PPP	IGS14	GipsyX v1.0	GPS only	Not applied
GR	GIANT-REGAIN (TUD, UTAS, OSU, NEWC)	Combination of 4 solutions with PPP and DD	IGb14	Bernese v5.2, Gipsy v6.4, GAMIT/GLOBK v10.71 and v10.70	GPS only	NTAL applied
TUD	Technical University of Dresden	DD (regional sites)	IGb14	Bernese v5.2	GPS only	Not applied
OSU	Ohio State University	DD (global sites)	IGb14	GAMIT/GLOBK v10.71	GPS only	Not applied

https://doi.org/10.5194/egusphere-2025-5358
Preprint. Discussion started: 7 November 2025

As shown in Table 1, the datasets were processed with distinct methodologies and rely on different realizations of the ITRF. NGL uses IGS14, GR uses IGb14, and AY uses IGS20. These are GNSS-specific realizations aligned with ITRF2014 (IGS14 and IGb14) and ITRF2020 (IGS20), respectively (Liu et al., 2021; Rebischung et al., 2024). While IGb14 is a refinement of IGS14 that includes updated station metadata and antenna calibrations, IGS20 is based on the ITRF2020, which benefits from a longer time series and improved modelling. ITRF2020 is aligned with ITRF2014 through a 14-parameter Helmert transformation derived from 131 globally distributed reference stations (Altamimi et al., 2023). The resulting differences, approximately 1.6–3.4 mm in position and 0.1–0.3 mm/yr in velocity, are small but can still affect long-term trend estimates if not consistently accounted for across datasets.

The NGL dataset was generated using precise point positioning (PPP) in GipsyX v1.0 with carrier-phase ambiguity resolution based on Jet Propulsion Laboratory's (JPL) WLPB (Wide-Lane Phase Bias) products (Blewitt et al., 2018; Gobron et al., 2021). Processing retained only Global Positioning System (GPS) data, excluding L2C/C2 observations. Atmospheric delays were modelled with Vienna Mapping Function 1 (VMF1) and ECMWF (European Centre for Medium-Range Weather Forecasts) grids, and ionospheric effects were corrected up to second order using IONEX (ionosphere exchange) and IGRF12 (International Geomagnetic Reference Field 12). Ocean and pole tide loading followed the IERS 2010 conventions with FES2004, while NTL was not applied. Station displacements were estimated using a stochastic Kalman filter in the IGS14 frame without applying a priori plate motion constraints.

The GR dataset was constructed by merging four independently processed GNSS solutions contributed by the GIANT-REGAIN project partners. Each group used different software and strategies to process the data, after which the solutions were aligned using Helmert transformations and combined station by station with weighted averages (Buchta et al., 2025c). NTAL was accounted for in the combination solution, but the individual TUD and OSU solutions were also obtained without NTAL applied.

TUD applied a network-based double-difference (DD) strategy using Bernese GNSS Software v5.2 (Buchta et al., 2025c). Antarctic stations were processed along with selected International GNSS Service (IGS) sites using final orbit and Earth rotation products from CODE (Centre for Orbit Determination in Europe). Atmospheric delays were estimated with the VMF3 mapping function using 1-hour zenith tropospheric delays (ZTD) and daily gradients. CODE global ionosphere maps (GIMs) products were used to model ionospheric delays up to third order. FES2014 ocean tide loading and atmospheric tide corrections from Ray and Ponte were applied, while NTL was excluded. Solid Earth and pole tide corrections followed IERS2010 standards. Ambiguities were resolved using a baseline-dependent strategy, and the IGb14 frame was realized using a no-net-translation (NNT) constraint with a core set of IGS stations.

OSU used DD processing in GAMIT/GLOBK v10.71, parallelised using the Parallel.GAMIT framework on high performance computing (HPC) infrastructure (Buchta et al., 2025c). IGS14 final orbits were applied. VMF1 gridded products were applied as a priori information for the zenith hydrostatic and wet delays, while GAMIT estimated the ZTD as a stochastic parameter using piecewise linear constrains with 1-hour resolution. Ocean tidal loading was corrected using FES2014b. Antarctic stations were processed within a Southern Hemisphere regional network, divided into sub-networks of approximately 40 stations, each

https://doi.org/10.5194/egusphere-2025-5358
Preprint. Discussion started: 7 November 2025

including a backbone of around 50 stations for reference. Daily subnet solutions were combined using GLOBK. The IGb14 frame was realized using a regional approach that constrained position, velocity, and seasonal signals with 60 core IGb14 stations.

The AY dataset was processed using undifferenced PPP with GipsyX v2.3, applying ionosphere-free linear combinations of carrier phase (LC) and pseudorange (PC) observations at 5-minute intervals and second-order ionospheric corrections applied with IONEX and IGRF12. JPL final orbits and clock products were used, with a priori tropospheric delays were obtained from the Vienna Mapping Function 1 (VMF1) grids (Böhm et al., 2006). The hydrostatic and wet zenith delays were mapped to the observation elevations using VMF1. The temporal variability of the zenith tropospheric delay was represented by a stochastic random-walk process with a process noise of $1.0 \times 10^{-5} m/\sqrt{sec}$. Tidal corrections included solid Earth, ocean (FES2004), and pole tides, following IERS 2010 conventions. Ambiguities were resolved with WLPB products, and daily station positions were estimated with a stochastic Kalman filter using a square root information smoother. Coordinates were transformed into the IGS20 reference frame, and final solution is in the centre of figure (CF) frame.

2.2 Non-tidal loading data

NTL data from two Earth system modelling groups, EOST (École & Observatoire des Sciences de la Terre, Strasbourg) and ESMGFZ (Earth System Modelling Group of GeoForschungsZentrum, Potsdam), were obtained and used in this study. Both groups provide displacement time series for NTAL, NTOL, and HYDL, computed using Green's functions following Farrell (1972). However, the groups differ in their choice of Earth models and source datasets. EOST calculates Green's functions based on the PREM (Preliminary Reference Earth Model) Earth model (Dziewonski and Anderson, 1981), as reported by Mémin et al. (2020). ESMGFZ uses the elastic Earth model "ak135" (Kennett et al., 1995), as described in Dill and Dobslaw (2013). All NTL displacement time series were obtained in the CF frame and were resampled to daily resolution by daily averaging.

For NTAL, the EOST dataset includes models based on ERA5 with inverse barometer (IB) corrections (ERA5IB), the TUGO-m (Toulouse Unstructured Grid Ocean model) barotropic model, as well as the MERRA-2 (The Modern-Era Retrospective analysis for Research and Applications, v2) reanalysis (Boy, 2021; Gelaro et al., 2017; Mémin et al., 2020). ESMGFZ provides NTAL based on the ECMWF operational forecast model, with atmospheric tides removed using harmonic analysis (Dill and Dobslaw, 2013; Dill et al., 2022). For NTOL, EOST uses the baroclinic ECCO2 (Estimating the Circulation and the climate of the Ocean, v2) ocean model (Mémin et al., 2020; Menemenlis et al., 2008), which does not include atmospheric pressure forcing. On the other hand, ESMGFZ relies on the MPIOM (Max Planck Institute Ocean Model) model (Jungclaus et al., 2013; Shihora et al., 2022a), which includes dynamic coupling with sea ice and Antarctic ice shelf cavities.

For HYDL, ESMGFZ uses the LSDM (Land Surface Discharge Model) model (Dill and Dobslaw, 2013; Dill et al., 2022), which includes surface water, snow, and runoff. EOST HYDL models were excluded due to their removal of permanently ice-covered regions, such as Antarctica, making them unsuitable for this study. Although LSDM provides global coverage, including Antarctica, it is important to recognize that current HYDL models remain highly uncertain in polar regions. In

https://doi.org/10.5194/egusphere-2025-5358
Preprint. Discussion started: 7 November 2025

Antarctica, seasonal hydrological signals are expected due to snow accumulation and melt, but existing HYDL models exhibit large inter-model inconsistencies and often lack precision metadata, making external validation necessary (Li et al., 2025). Moreover, HYDL models, including LSDM, do not explicitly incorporate glacial processes (e.g., ice dynamics or ice mass discharge), which are key drivers of surface loading in Antarctica (Poropat et al., 2019). A summary comparison of the models and processing approaches used by each group is presented in Table 2.

Table 2: Comparison of ESMGFZ and EOST NTL models and processing characteristics.

Aspect	*EOST*	*ESMGFZ*
NTAL model	ERA5IB (0.25˚, 1h), MERRA-2 (0.625˚, 1h), TUGO-m (0.25˚, 3h)	ECMWF operational model (0.5˚, 3h)
NTAL tide removal	IB correction (ERA5IB, MERRA-2), dynamic response (TUGO-m)	Harmonic analysis of wind and pressure components
NTOL model	ECCO2 (0.25˚, daily), baroclinic; no atmospheric pressure forcing	MPIOM (1.0˚, 3h); dynamic ocean forced by ECMWF
NTOL tide removal	Dynamic ocean model or IB assumption	Harmonic removal of 12 constituents (currents + bottom pressure)
HYDL model	not used; ice-covered areas excluded	LSDM (0.5˚, daily)
Earth model	PREM	ak135 elastic Earth model
Reference Frame	CF	CF
Output Resolution	0.25˚ - 1˚ (depends on model)	Final output: 0.5˚; internal: 0.125˚ (near), 2.0˚ (far)
Coverage of Polar regions	All NTAL models are global and include polar regions; ECCO2 includes sea-ice model; HYDL models don't cover permanently ice-covered areas	NTAL and HYDL models are global and include polar regions; NTOL model includes sea-ice components and Antarctic ice-shelf cavities
Mass conservation handling	Uniform land-ocean mass balancing	Boussineq correction for ocean bottom pressure

3 Methodology

This study evaluates the impact of NTL corrections on GNSS timeseries using the Hector 2.1 software (Bos et al., 2013). The analyses focus on trends, seasonal signals and noise characteristics. Since the GNSS time series varied in length, a common starting date of 1.2.2003, the first day present in all datasets, was selected. This analysis results in approximately 18 years of continuous data, sufficient to resolve long-term trends and multiple seasonal cycles, thereby enhancing the robustness of the noise and signal estimates.

To ensure consistency across all datasets, GNSS station positions were converted from geocentric Cartesian coordinates (XYZ) to local topocentric Cartesian coordinates (ENU). Coordinate differences relative to the first epoch were calculated following Eq. (1):

$$\Delta X = X_i - X_0,\ \ \Delta Y = Y_i - Y_0,\ \ \Delta Z = Z_i - Z_0 \quad (1)$$

https://doi.org/10.5194/egusphere-2025-5358
Preprint. Discussion started: 7 November 2025

where X_i, Y_i, Z_i are the Cartesian coordinates at epoch i, and X_0, Y_0, Z_0 are the reference Cartesian coordinates from the first epoch. These differences were then transformed into ENU displacements using a rotation matrix based on each station's geodetic latitude ϕ and longitude λ following Eq. (2). This approach ensures that displacements are defined relative to a common topocentric frame across all datasets.

$$\begin{bmatrix} E \\ N \\ U \end{bmatrix} = \begin{bmatrix} -sin\lambda & cos\lambda & 0 \\ -sin\phi cos\lambda & -sin\phi sin\lambda & cos\phi \\ cos\phi cos\lambda & cos\phi sin\lambda & sin\phi \end{bmatrix} \begin{bmatrix} \Delta X \\ \Delta Y \\ \Delta Z \end{bmatrix} \quad (2)$$

The resulting displacements were expressed in millimetres. To correct for loading effects, NTL data was requested from the EOST and ESMGFZ repositories in the CF frame. The raw GNSS time series were adjusted by subtracting the corresponding loading displacements. No NTAL corrections were applied to the GR dataset, as these corrections were already included during initial processing (Buchta et al., 2025c). The types and combinations of NTL corrections are summarised in Table 3. Each combination was applied separately, and individual files were generated for both the uncorrected and corrected data for each station and displacement component.

Table 3: Summary of applied NTL correction combinations.

Referred as	*NTL type*	*Correction model*	*Provider*
EOST1	NTAL	ERA5IB	EOST
EOST2	NTAL	MERRA2	EOST
GFZ1	NTAL	ECMWF	ESMGFZ
EOST3	NTAL + NTOL	ERA5TUGO-m	EOST
EOST4	NTAL + NTOL	ERA5IB + ECCO2	EOST
EOST5	NTAL + NTOL	MERRA2 + ECCO2	EOST
GFZ2	NTAL + NTOL	ECMWF + MPIOM	ESMGFZ
GFZ3	NTAL + NTOL + HYDL	ECMWF + MPIOM + LSDM	ESMGFZ
EOST6	NTOL	ECCO2	EOST
GFZ4	NTOL	MPIOM	ESMGFZ
GFZ5	NTOL + HYDL	MPIOM + LSDM	ESMGFZ

Time series modelling was conducted using the Power-Law + White Noise (PLWN) noise model in Hector. For each uncorrected and corrected time series, Hector estimated trends, seasonal amplitudes, and noise characteristics were obtained by running the scripts provided by Bos et al. (2013). Offsets were accounted for based on the log files provided by Buchta et al. (2025a). The PLWN model was selected as it accurately captures the temporal correlations typically present in GNSS position series, which arise from a combination of geophysical, instrumental, and environmental factors. As noted by

https://doi.org/10.5194/egusphere-2025-5358
Preprint. Discussion started: 7 November 2025

Hohensinn et al. (2024), inadequate stochastic modelling, particularly of low-frequency noise, can substantially bias estimates of station velocity and its uncertainty. Numerous studies have shown that PLWN provides a realistic representation of GNSS time series noise (Bevis et al., 2020; Bos et al., 2010; Gobron et al., 2024; He et al., 2019; Klos et al., 2017; Williams et al., 2004).

Following Hector analysis, displacement residuals were calculated by subtracting the observed positions from the modelled displacements. To assess the impact of loading corrections, both root mean square (RMS) and weighted root mean square (WRMS) of the residuals were calculated before and after applying the corrections. These metrics were calculated separately for the east, north, and up components, using the following formulas Eq. (3) and Eq. (4) as also outlined in Ejigu et al., (2024):

$$RMS = \sqrt{\frac{1}{N}\sum_{i=1}^{N} Ts_i^2} \tag{3}$$

$$WRMS = \sqrt{\frac{1}{N-1}\frac{\sum_{i=1}^{N}\left(\frac{(Ts_i-\overline{Ts_\iota})^2}{\sigma_i^2}\right)}{\sum_{i=1}^{N}\sigma_i^2}} \tag{4}$$

where Ts_i is the daily coordinate displacement solution, N is the total number of observations, σ_i is the formal error, and $\overline{Ts_\iota}$ is the weighted average calculated as Eq. (5):

$$\overline{Ts_\iota} = \frac{\sum_{i=1}^{N}\frac{Ts_i}{\sigma_i^2}}{\sum_{i=1}^{N}\frac{1}{\sigma_i^2}} \tag{5}$$

To quantify the effectiveness of each loading correction, the relative change in RMS and WRMS was expressed as a percentage using the following formula Eq. (6):

$$Change\ (\%) = \left(\frac{Original - Corrected}{Original}\right) \times 100\% \tag{6}$$

Positive values indicate a reduction (i.e., improved model fit), while negative values indicate an increase in RMS or WRMS. This analysis was carried out separately for each correction model, station, and GNSS dataset. In addition, Hector provided uncertainty estimates for linear trends and seasonal amplitudes, accounting for the noise model used.

https://doi.org/10.5194/egusphere-2025-5358
Preprint. Discussion started: 7 November 2025

4 Results

The effectiveness of the NTL corrections in improving data quality was assessed by examining RMS values and Hector-estimated parameters, including trends, spectral indices, noise components (PL and WN), and seasonal amplitudes. The main objective of this analysis was to determine how the 11 different NTL correction model combinations, along with GNSS datasets with different processing strategies affect the stability and accuracy of the time series. The results indicate significant differences between different datasets, both prior and following the application of corrections.

4.1 Comparison of uncorrected GNSS datasets

Before assessing the impact of NTL corrections, it is important to understand the behaviour of the uncorrected GNSS time series. This provides a reference against which the effect of loading corrections can be evaluated and offers insights into how processing strategies and underlying assumptions influence estimated trends, seasonal amplitudes and noise characteristics. Such differences can impact the interpretation of geophysical signals, such as crustal motion or GIA.

Figure 2 presents the uncorrected vertical displacement time series for the five datasets at each station. Among the stations, SYOG provides the most continuous record with relatively few gaps. In contrast, ABOA shows longer data gaps in 2006 and 2021, while VESL has interruptions around 2007, 2009, and 2013. In terms of apparent long-term behaviour, ABOA shows a quite even trend, SYOG a slight downward trend likely caused by the offsets, while VESL appears to rise during the first half of the record and then subside in later years. Across the datasets, the GR solution exhibits the least variation and smoothest time series. In comparison, the AY, NGL, OSU, and TUD datasets display higher variation, stronger seasonal oscillations, and increased sensitivity to offsets and seasonal variability.

https://doi.org/10.5194/egusphere-2025-5358
Preprint. Discussion started: 7 November 2025

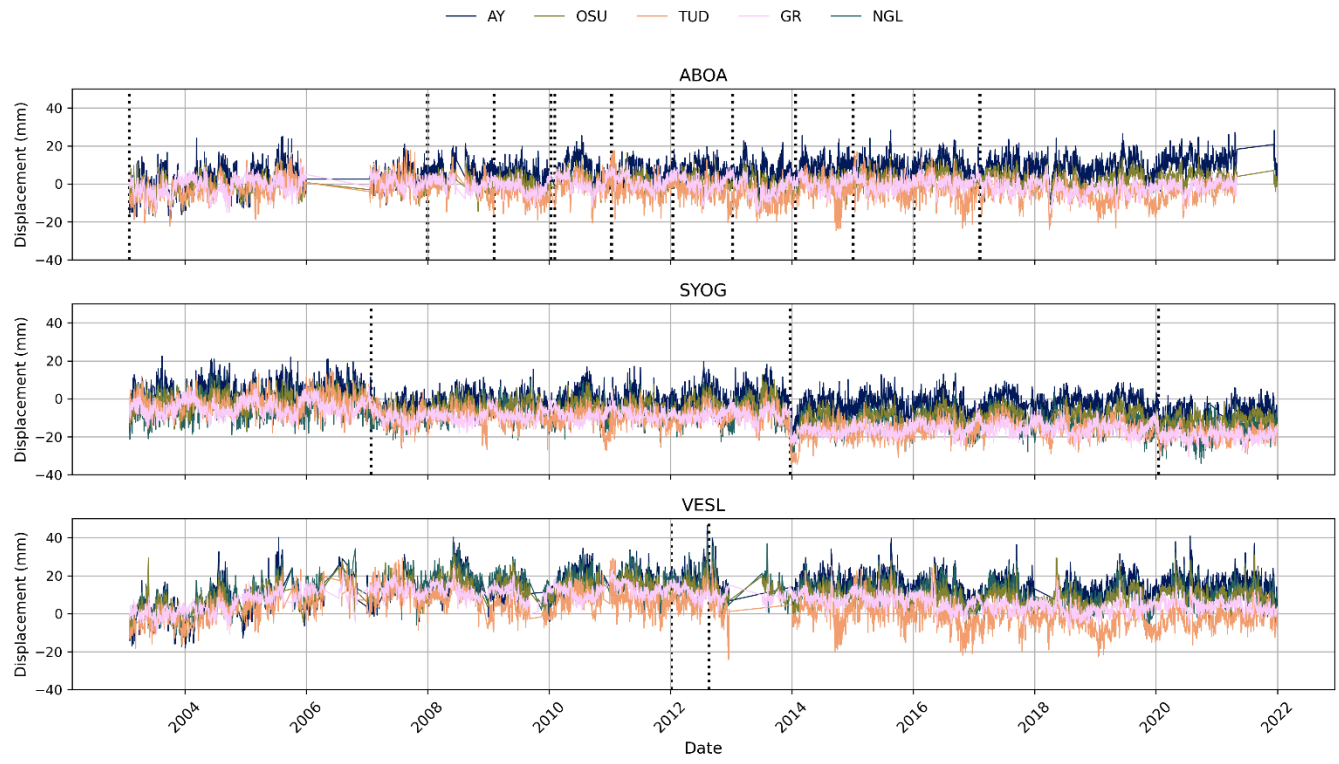

Figure 2: Uncorrected vertical displacement time series for five GNSS datasets (AY, NGL, OSU, TUD, GR) at each station (ABOA, SYOG, VESL; top to bottom). Black dotted lines indicate offsets considered during processing. Axes are plotted using a consistent scale.

Closer inspection of the Hector-estimated parameters (Figure 3) reveals substantial variability between datasets in vertical trends, noise, and seasonal amplitudes. For example, at SYOG (middle column of each subplot in Figure 3), the uplift rates vary from 0.53 ± 0.16 mm/yr in the GR solution to 1.10 ± 0.23 mm/yr in the AY solution. Noise spectra at SYOG are dominated by a mixture of white and flicker noise, with spectral indices typically between –0.8 and –0.98. PL amplitudes exceed WN amplitudes in all cases, with SYOG generally showing the lowest PL amplitudes. Exceptions are the TUD and GR datasets, with PL amplitudes of 12.45 $mm/yr^{\hat{\kappa}/4}$ and 7.65 $mm/yr^{\hat{\kappa}/4}$, respectively, and corresponding WN amplitudes of 1.44 mm and 0.81 mm. In other datasets, WN amplitudes are close to zero, while PL amplitudes are around 12 – 14 $mm/yr^{\hat{\kappa}/4}$. Seasonal cycles also differ: TUD shows the weakest annual (1.32 ± 0.36 mm) and semi-annual (0.55 ± 0.24 mm) signals, while other datasets yield annual amplitudes of ~2.1 – 2.8 mm and semi-annual amplitudes near 1 mm.

https://doi.org/10.5194/egusphere-2025-5358
Preprint. Discussion started: 7 November 2025

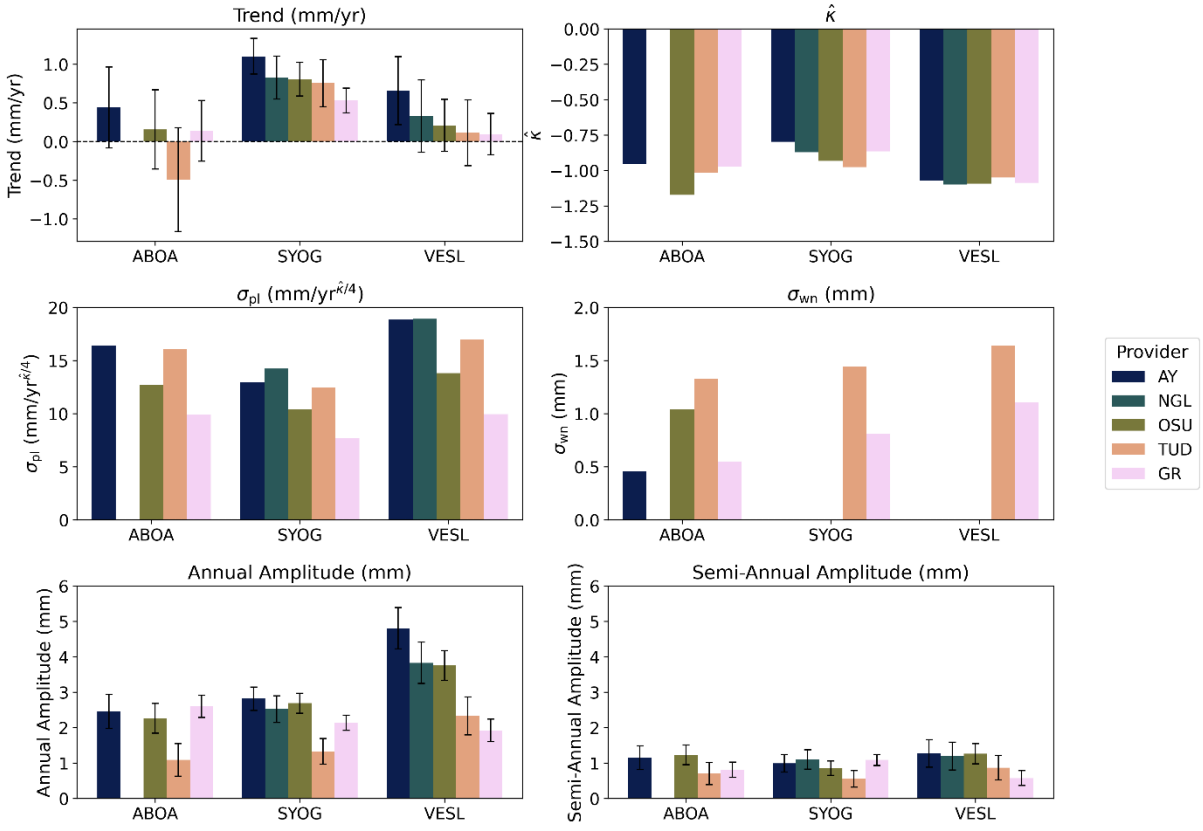

Figure 3: Comparison of Hector-estimated parameters across stations and datasets: vertical trends (upper left), spectral index $\hat{\kappa}$ (upper right), PL amplitude (middle left), WN amplitude (middle right), annual amplitude (bottom left), and semi-annual amplitude (bottom right). The WN amplitudes of AY, NGL, and OSU are close to zero at SYOG and VESL. The scales vary between different metrics.

At ABOA (left column of each subplot in Figure 3), trends are smaller overall. The TUD dataset shows a negative vertical trend (–0.49 ± 0.67 mm/yr), while AY yields the most positive trend (0.44 ± 0.52 mm/yr). Noise levels are generally higher than at SYOG: spectral indices are close to –1.0, and PL amplitudes are large. The AY dataset has the highest PL amplitude (16.42 $mm/yr^{\hat{\kappa}/4}$) and the lowest WN amplitude (0.46 mm), whereas the TUD dataset has one of the highest PL (16.08 $mm/yr^{\hat{\kappa}/4}$) and WN amplitudes (1.32 mm). Seasonal amplitudes are comparable to those at SYOG, with annual amplitudes exceeding 2 mm and semi-annual amplitudes around 1 mm.

VESL (right column of each subplot in Figure 3) exhibits the greatest variability between datasets. The AY dataset stands out with a relatively strong positive vertical trend (0.65 ± 0.44 mm/yr), while GR is nearly even (0.09 ± 0.27 mm/yr). Noise spectra are similar across datasets, with $\hat{\kappa}$ values approximately –1.0. Both PL and WN amplitudes are larger than at SYOG or ABOA: NGL shows the largest PL amplitude (18.91 $mm/yr^{\hat{\kappa}/4}$), while TUD has the highest WN amplitude (1.64 mm). Seasonal signals are also more variable. AY shows the strongest annual amplitudes (4.80 ± 0.58 mm), while TUD and GR have weaker

https://doi.org/10.5194/egusphere-2025-5358
Preprint. Discussion started: 7 November 2025

annual amplitudes (TUD: 2.33 ± 0.54 mm; GR: 1.91 ± 0.32 mm). The semi-annual amplitudes are relatively consistent across datasets.

Overall, the reference solutions reveal notable variability across stations and processing strategies. The GR dataset consistently exhibits lower PL amplitudes and more stable trend and seasonal signal estimates. This is likely attributable to two factors: first, the GR dataset is a combination of four independent solutions, which reduces random noise through ensemble averaging; second, it includes prior NTAL corrections, which already mitigate some transient environmental effects. However, while this combination strategy improves signal stability, it may also smooth out localized geophysical signals present in individual solutions. In contrast, the AY, NGL, TUD, and OSU datasets exhibit larger PL and seasonal amplitudes in the uncorrected time series. Elevated PL amplitudes indicate stronger long-term correlations, which inflate uncertainty in velocity and seasonal terms. On the other hand, WN amplitudes, particularly in TUD and GR, primarily indicate short-term scatter and have limited impact on long term trends.

In addition, vertical trend estimates occasionally differ between datasets by more than their formal uncertainty bounds. These discrepancies likely arise from differences in processing strategies, reference frame realizations, and the application or absence of a priori corrections (Table 1). As such, they directly influence the reliability of trend and seasonal signal estimates, with implications for interpreting crustal deformation and surface mass loading in Antarctica. The observed discrepancies also raise a critical question: which dataset most accurately represents geophysical reality? As seen here, in some cases, even the direction of vertical crustal motion differs between datasets, with different solutions indicating either uplift or subsidence at the same station. Although often within error margins, these discrepancies are important for applications such as GIA model verification, where both the sign and magnitude of vertical trends are decisive.

4.2 Impact of loading corrections on GNSS time series

The application of NTL corrections to GNSS time series affected vertical displacement trends, seasonal amplitudes, and noise characteristics across all datasets. However, the magnitude and direction of these effects depend strongly on the station location, processing strategy, and specific correction model applied. This section presents a comparative analysis of three Antarctic GNSS stations (ABOA, SYOG, VESL) using five datasets (AY, NGL, OSU, TUD, GR) and 11 different model combinations. The focus is on evaluating correction effectiveness through vertical trends, seasonal signals, noise, and RMS metrics derived from Hector outputs. Full Hector results are presented in Appendix A, while RMS values are compiled in Appendix B.

4.2.1 Vertical displacement trends

Vertical displacement rates are sensitive to NTL corrections, although the direction and magnitude of change vary by station, dataset and correction model. These variations are illustrated in Figure 4, which compares the impact of NTL corrections on vertical trends for ABOA, SYOG, and VESL.

https://doi.org/10.5194/egusphere-2025-5358
Preprint. Discussion started: 7 November 2025

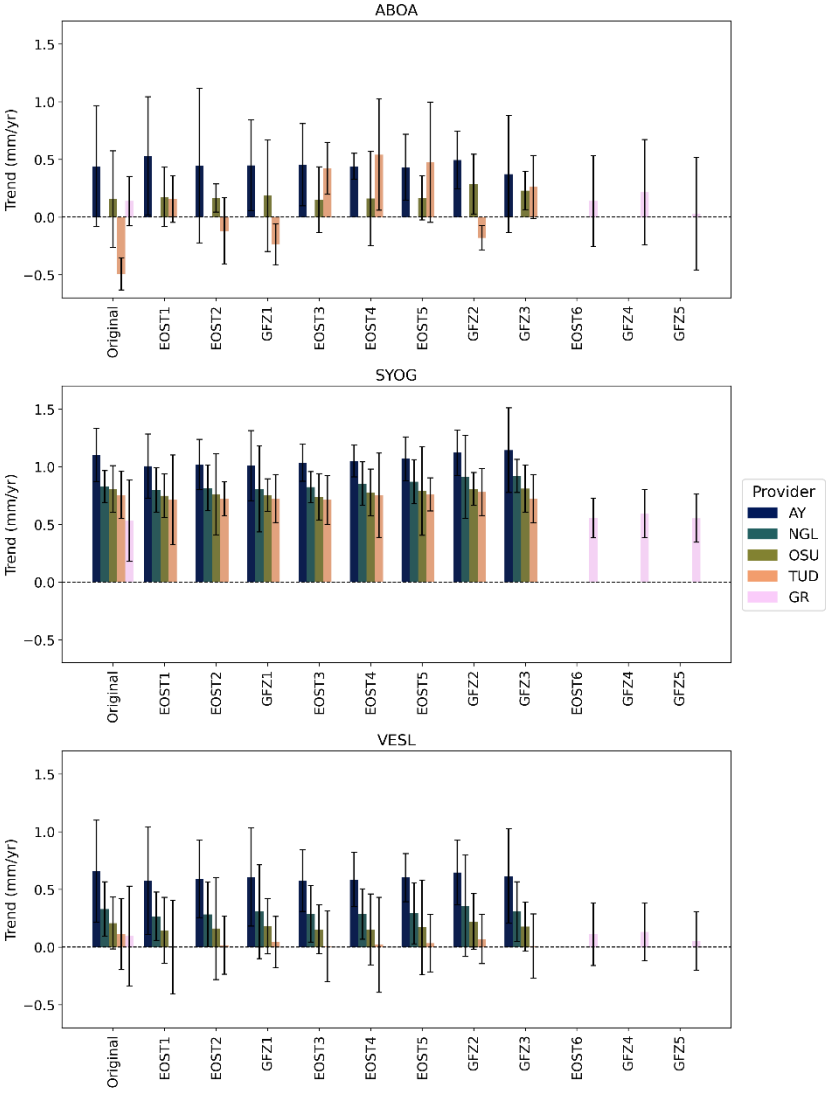

Figure 4: Effect of NTL corrections on vertical displacement trends at ABOA (top), SYOG (middle), and VESL (bottom). Each panel shows trend estimates for different datasets and correction models, allowing direct comparison of correction sensitivity across stations. For each dataset, the uncorrected trend is shown first, followed by NTAL, NTAL + NTOL, NTAL + NTOL + HYDL, and the GR-specific corrections. All values are shown as absolute trends, and a consistent vertical axis scale is used to facilitate inter-station comparison.

At ABOA, vertical trends are generally stable across correction models, with modest sensitivity to loading effects. In the AY dataset, the uncorrected trend is 0.44 ± 0.52 mm/yr, and most corrections keep values within 0.43 – 0.53 mm/yr. An exception occurs with GFZ3, which reduces the rate to 0.37 ± 0.11 mm/yr. In contrast, the TUD dataset exhibits larger variability. The uncorrected rate of –0.49 ± 0.67 mm/yr is increased with all corrections. For example, EOST4 changes the sign of the rate, yielding uplift of 0.54 ± 0.14 mm/yr, whereas GFZ1 increases it more modestly to –0.24 ± 0.48 mm/yr.

https://doi.org/10.5194/egusphere-2025-5358
Preprint. Discussion started: 7 November 2025

At SYOG, vertical trends are dataset dependent but relatively stable in magnitude. The AY dataset consistently has the largest uplift, with the uncorrected value of 1.10 ± 0.23 mm/yr reduced under most corrections to ~1.0 mm/yr, except GFZ2 and GFZ3, which increases it slightly to ~1.13 mm/yr. In the NGL dataset, corrections generally increase uplift, from 0.83 ± 0.28 mm/yr to ~0.91 mm/yr with GFZ2 and GFZ3. The OSU dataset follows a similar pattern, with uncorrected uplift of 0.81 ± 0.22 mm/yr decreasing slightly under NTAL-only corrections but returning to ~0.81 mm/yr with GFZ2 and GFZ3. In contrast, TUD consistently yields lower uplift than other datasets, with values around 0.71 – 0.78 mm/yr. Across datasets, corrections at SYOG tend to reduce formal uncertainties in the PPP-processed datasets, and GFZ models in particular often enhance uplift relative to uncorrected series.

At VESL, vertical trends resemble ABOA in their large uncertainties and modest sensitivity to corrections. All datasets indicate uplift, although uncertainties are sufficiently large that subsidence cannot be excluded. The AY dataset shows the highest uplift, with the original trend of 0.66 ± 0.44 mm/yr decreasing under corrections to ~0.58 – 0.65 mm/yr. In the NGL dataset, uplift rates decrease from 0.33 ± 0.47 mm/yr to ~0.27 – 0.36 mm/yr under most corrections, while in OSU values are lowered from 0.21 ± 0.34 mm/yr to ~0.15 – 0.22 mm/yr. In the TUD dataset, uplift nearly vanished, with the uncorrected rate of 0.11 ± 0.43 mm/yr reduced to ~0.00 – 0.07 mm/yr. Overall, at VESL corrections typically reduce uplift and uncertainties, though the effect varies in magnitude across datasets.

Overall, NTL corrections have a variable impact on vertical displacement trends, depending on the dataset, station, and correction model. Corrections applying NTAL alone generally have modest effects, often slightly reducing the trend magnitude. The addition of NTOL tends to introduce larger shifts and, in some cases, reverse the sign of the rate, as observed at ABOA. The inclusion of HYDL seems to generally increase uplift rates. The effects on the GR dataset remain modest, but corrections including HYDL still induce noticeable shifts (e.g., at ABOA from 0.14 ± 0.39 mm/yr to 0.03 ± 0.49 mm/yr). Thus, the results show that NTL corrections do not have uniform effects across Antarctica and that their influence depends on both the choice of dataset and the combination of loading components applied.

4.2.2 Seasonal amplitude changes

NTL corrections also affect the seasonal amplitude structure of GNSS time series. The changes vary slightly across stations and correction models, with annual amplitudes generally more sensitive than semi-annual amplitudes. These results are summarised in Figure 5, which separated annual and semi-annual amplitude responses.

https://doi.org/10.5194/egusphere-2025-5358
Preprint. Discussion started: 7 November 2025

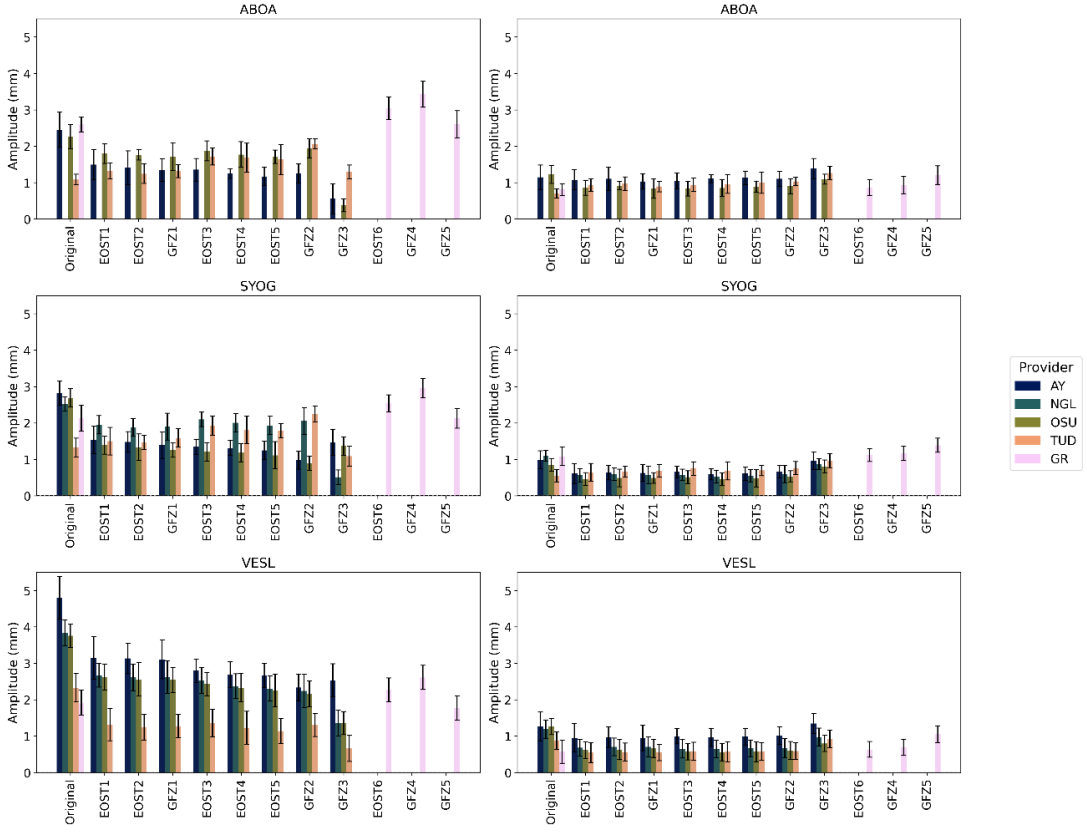

Figure 5: Effect of NTL corrections on seasonal amplitudes at ABOA (top), SYOG (middle), and VESL (bottom). The first column shows annual amplitudes and the second column semi-annual amplitudes. For each dataset, the uncorrected amplitude is shown first, followed by NTAL, NTAL + NTOL, NTAL + NTOL + HYDL, and the GR-specific corrections. All values are shown as absolute amplitudes, and a consistent vertical axis scale is used to facilitate inter-station comparison.

At ABOA, most corrections reduce the vertical annual amplitude, especially in the AY and OSU datasets. For example, the AY dataset's annual amplitude decreases from 2.46 ± 0.48 mm to 0.55 ± 0.14 mm under GFZ3, while OSU decreases from 2.26 ± 0.42 mm to 0.38 ± 0.19 mm with the same correction. In contrast, the TUD and GR datasets generally show increased annual amplitudes post-correction (e.g., TUD: from 1.09 ± 0.46 mm to 2.06 ± 0.41 mm). Semi-annual amplitudes are smaller (typically ~0.7 – 1.1 mm) and remain relatively stable across corrections, with only modest changes.

At SYOG, similar patterns are observed, with most datasets exhibiting reduced annual amplitudes after corrections. The largest decreases occur in the AY, NGL, and OSU datasets under GFZ2 and GFZ3. For instance, AY decreases from 2.81 ± 0.33 mm to 0.98 ± 0.19 mm with GFZ2, while NGL decreases 2.52 ± 0.38 mm to 0.51 ± 0.22 mm with GFZ3. In contrast, the TUD and GR datasets often show amplification: GFZ2 increases the TUD annual amplitude 1.33 ± 0.36 mm to 2.25 ± 0.38 mm, while GFZ4 increases GR from 2.13 ± 0.21 mm to 2.96 ± 0.27 mm. Semi-annual amplitudes remain comparatively stable, although slight increases occur in GR and TUD.

At VESL, annual amplitudes are generally larger than at ABOA and SYOG, but corrections effectively reduce them in all datasets except GR. For example, the NGL dataset decreases from 3.82 ± 0.59 mm to 1.36 ± 0.31 mm with GFZ3, while OSU

https://doi.org/10.5194/egusphere-2025-5358
Preprint. Discussion started: 7 November 2025

drops from 3.75 ± 0.42 mm to 1.36 ± 0.36 mm under the same correction. In AY, annual amplitudes decline from 4.80 ± 0.58 mm to 2.34 ± 0.35 mm with GFZ2, and even TUD decreases from 2.33 ± 0.54 mm to 0.65 ± 0.34 mm with GFZ3. Semi-annual amplitudes are smaller (typically ~0.6 – 1.3 mm) and decrease after most corrections, although the GR dataset again shows minor increases.

Overall, annual amplitudes are more responsive to NTL corrections than semi-annual amplitudes. The inclusion of NTOL and HYDL tends to enhance the reduction of annual amplitudes, but in many cases, it leads to larger semi-annual amplitudes. However, these effects are not uniform: in the GR and TUD datasets, seasonal amplitudes often increase at ABOA and SYOG, and at VESL the GR dataset could not be improved. Among the three stations, ABOA and SYOG generally achieve smaller corrected seasonal amplitudes, while VESL retains the largest seasonal signal even after correction. Phase shits between stations and datasets also vary, with most seasonal peaks occurring between late austral winter and early austral autumn (August to March). The addition of HYDL generally has the strongest impact on the phase.

4.2.3 Noise characteristics

Noise levels in the vertical component are an important metric for evaluating the effectiveness of corrections. Figure 6 illustrates $\hat{\kappa}$, PL amplitude, and WN amplitude for each dataset and correction. These three parameters together indicate the relative contribution of temporally correlated and uncorrelated noise to the time series.

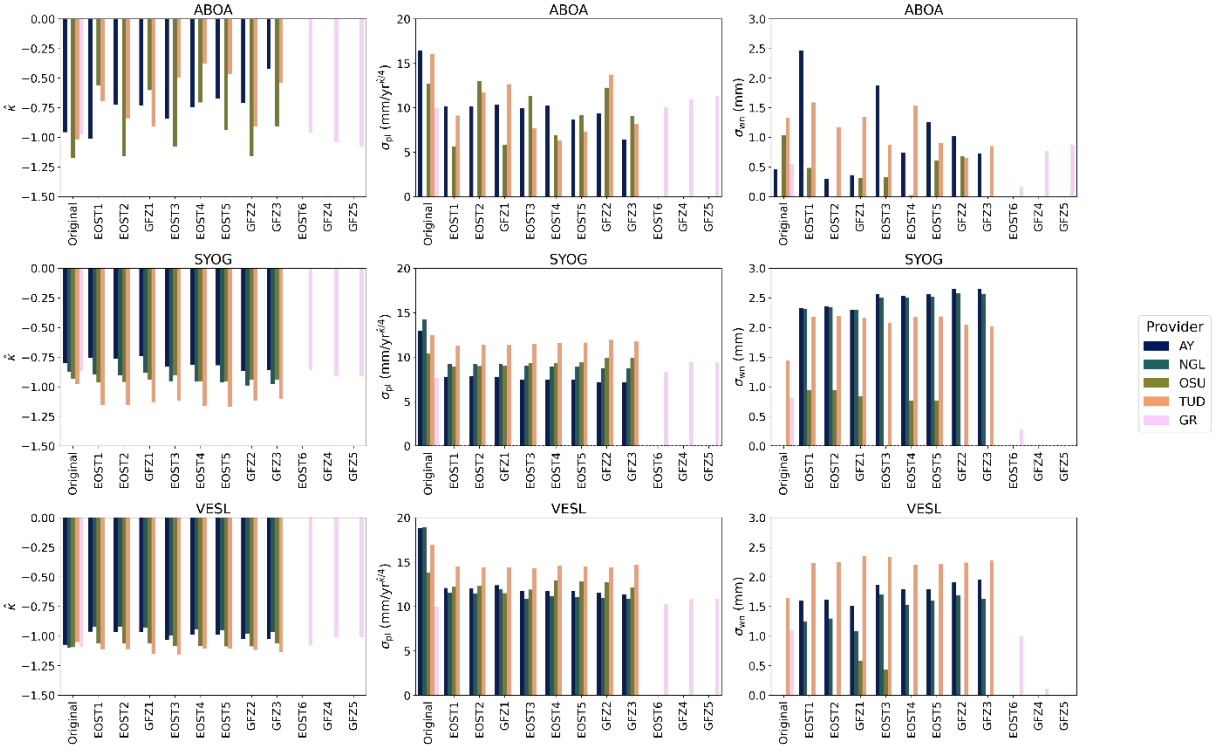

Figure 6: Effect of NTL corrections on noise levels at ABOA (top), SYOG (middle), and VESL (bottom). For each dataset, the uncorrected noise is shown first, followed by NTAL, NTAL + NTOL, NTAL + NTOL + HYDL, and the GR-specific corrections. All values are shown as absolute noise, and a consistent vertical axis scale is used to facilitate inter-station comparison.

https://doi.org/10.5194/egusphere-2025-5358
Preprint. Discussion started: 7 November 2025

At ABOA, uncorrected time series typically show high PL amplitudes (e.g., AY: 16.42 $mm/yr^{\hat{\kappa}/4}$; TUD: 16.08 $mm/yr^{\hat{\kappa}/4}$) consistent with strong low-frequency noise, and moderate WN levels (0.5 – 1.3 mm). Corrections generally reduce the PL amplitude with the most effective depending on the dataset (e.g., GFZ3 for AY: 6.41 $mm/yr^{\hat{\kappa}/4}$; EOST4 for TUD: 6.32 $mm/yr^{\hat{\kappa}/4}$). At the same time, corrections seem to reduce $\hat{\kappa}$ values in most datasets, except for GR. This indicates a relative shift toward less correlated noise. In contrast, the GR dataset retains high PL amplitudes ($\geq$ 10 $mm/yr^{\hat{\kappa}/4}$) with no improvement, suggesting corrections are less effective for this solution. WN amplitudes vary more strongly: some corrections introduce additional uncorrelated noise (e.g., AY EOST1: from 0.46 mm to 2.46 mm), while others reduce it substantially (e.g., OSU EOST2: from 1.04 mm to 0.009 mm).

At SYOG, uncorrected datasets also display large PL amplitudes (AY: 12.97 $mm/yr^{\hat{\kappa}/4}$; NGL: 14.24 $mm/yr^{\hat{\kappa}/4}$) with $\hat{\kappa}$ values near –1.0, characteristic of flicker noise. Corrections consistently reduce PL amplitudes, often to 7 – 9 $mm/yr^{\hat{\kappa}/4}$ under all corrections. The largest reductions are observed in AY (to 7.12 $mm/yr^{\hat{\kappa}/4}$) and NGL (to 8.74 $mm/yr^{\hat{\kappa}/4}$) with the GFZ3 corrections. WN amplitudes are generally higher than at other stations, and some corrections (e.g., AY EOST1–5) increase WN levels relative to the uncorrected time series, while others (OSU GFZ2–3) yield extremely low estimates. The spectral index remains relatively stable, although some corrections produce slightly flatter slopes, indicating a modest reduction in correlation strength.

At VESL, noise levels are the largest among the three stations. Uncorrected series exhibit the highest PL amplitudes (AY: 18.22 $mm/yr^{\hat{\kappa}/4}$; NGL: 18.91 $mm/yr^{\hat{\kappa}/4}$; TUD: 16.98 $mm/yr^{\hat{\kappa}/4}$). Corrections reduce PL amplitudes considerably, although values remain higher than at ABOA or SYOG. For example, AY decreases to 11.33 $mm/yr^{\hat{\kappa}/4}$ and NGL to 10.88 $mm/yr^{\hat{\kappa}/4}$ with GFZ3. OSU and TUD show more modest improvements (e.g., TUD to 14.40 $mm/yr^{\hat{\kappa}/4}$ with GFZ1). WN amplitudes at VESL are also higher, particularly for TUD (>2.0 mm after corrections), reflecting strong short-term scatter. The spectral index remains steep and lower than at other stations, consistent with dominant PL processes.

Overall, corrections generally reduce PL amplitudes across stations, with GFZ3 frequently providing the strongest improvements. WN amplitudes respond more inconsistently: in some cases, they increase as PL amplitudes decrease (e.g., ABOA AY EOST2), while in other cases, they also decrease. Spectral index values remain similar across all stations and datasets, with most changes occurring at ABOA. Among the three stations, ABOA and SYOG also show the most consistent improvement in both PL and WN noise after correction, while VESL retains the largest and most correlated noise even after corrections.

4.2.4 RMS improvement and correction efficiency

RMS values provide a comprehensive measure of residual variability and correction effectiveness. While WRMS values were also calculated, one dataset lacked formal error values, preventing full WRMS-based comparison. Given that both RMS and WRMS exhibited similar patterns across datasets, only RMS values are analysed in detail here. The vertical RMS values are shown in Figure 7, with full results provided in Appendix B.

https://doi.org/10.5194/egusphere-2025-5358
Preprint. Discussion started: 7 November 2025

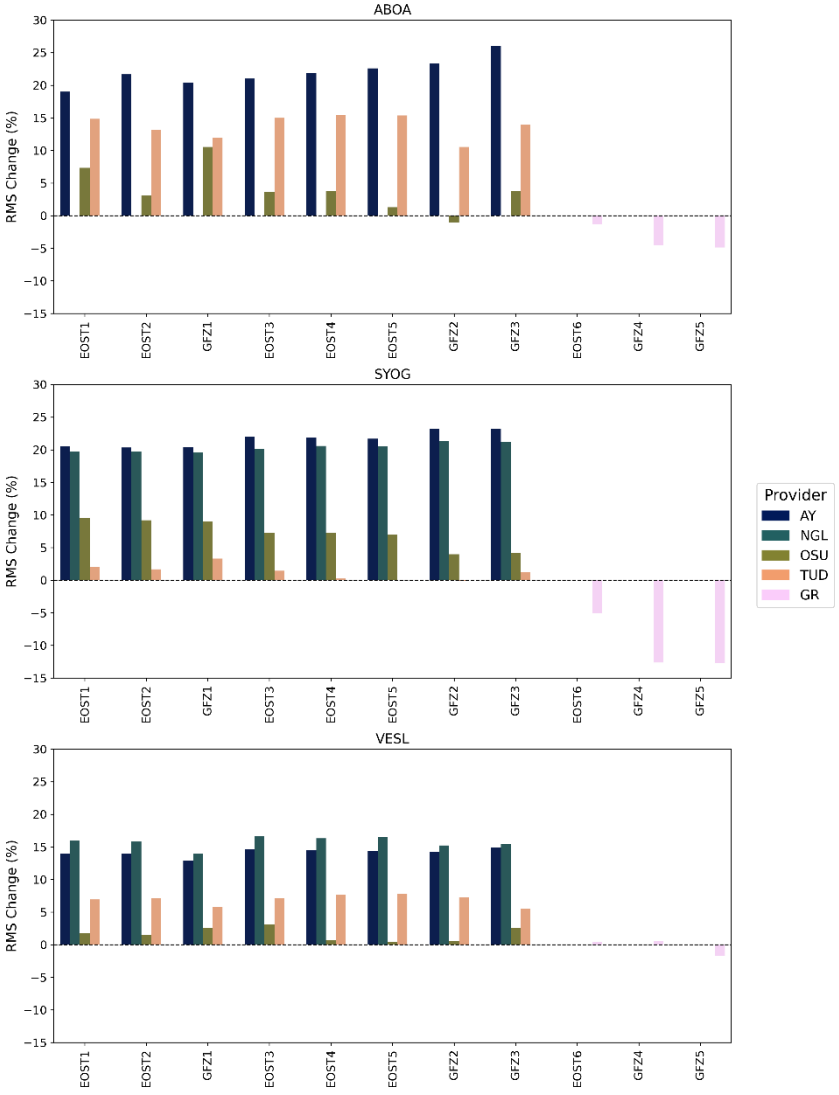

Figure 7: Effect of NTL corrections on RMS in the vertical component at ABOA (top), SYOG (middle), and VESL (bottom). Negative values indicate an increase in WRMS, while positive values indicate a reduction. All plots share the same vertical axis scale to facilitate inter-station comparison.

At ABOA, most corrections reduce vertical RMS, but the degree of improvement varies. The largest relative gains are observed in the AY dataset, where GFZ3 reduces RMS by 26.04 %, and most corrections including both NTOL and HYDL typically yield better results than those incorporating only NTAL. In contrast, the OSU and TUD datasets show more modest improvements (OSU: 3 – 10 %; TUD: 12 – 15 %), and in the case of GFZ2 in OSU, RMS degradation is observed (–1.05 %). The GR dataset displays no benefit from corrections, with RMS increasing by up to 4.89 % under GFZ5.

At SYOG, significant improvements occur in the AY and NGL datasets, particularly when using GFZ or EOST corrections with NTOL. The GFZ2 correction yielded the largest improvements, reducing RMS by 23.21 % in AY and 21.32 % in NGL. Meanwhile, the OSU, TUD, and GR datasets show limited or negative responses to corrections that are reduced with the

https://doi.org/10.5194/egusphere-2025-5358
Preprint. Discussion started: 7 November 2025

addition of NTOL and HYDL. For example, OSU shows moderate improvements overall (4 – 10 %), while TUD shows even more limited improvement (–0 – 3 %), with models including NTOL driving the change toward 0 %. The GR dataset benefits again the least form the corrections, with RMS increasing by over 12 % with GFZ models.

At VESL, AY and NGL again achieve the most substantial reductions across all corrections, with the NGL dataset benefitting slightly more from the corrections. Improvements reach 13 – 15 % in the AY dataset and 14 – 17 % in the NGL dataset, with GFZ3 and EOST3 providing the largest reductions. In contrast, corrections applied to the TUD, OSU, and GR datasets either show smaller improvements or increase RMS values (TUD: 5 – 8 %; OSU: 0 – 3 %; GR: –2 – 1 %).

Across stations, NTAL appears to have the largest impact on reducing RMS, while NTOL and HYDL provide smaller additional contributions. AY and NGL consistently show the largest RMS reductions at each station, whereas OSU and TUD exhibit more limited improvements. Interestingly, TUD performs better at ABOA and VESL, while OSU achieves larger improvements at SYOG. These differences are likely tied to the differing network strategies used. Both OSU and TUD are processed as network solutions using GAMIT and Bernese, respectively, which depend on the spatial distribution and quality of reference stations. In Antarctica, where the reference network is sparse and unevenly distributed, this can introduce additional spatial biases and reduce the effectiveness of NTL corrections.

In contrast, the better performance of PPP-processed datasets (AY and NGL) suggests that PPP may be more robust under these conditions, as it does not rely on a dense reference network and is less sensitive to errors in reference frame realization. This is also consistent with findings by He et al. (2017), who showed that Antarctic stations tend to exhibit higher WRMS values in DD solutions compared to PPP solutions. Further differences in reference frame realization likely also contribute to the varying performance across datasets. For example, according to Buchta et al. (2025c), the OSU solution uses globally distributed IGS reference sites, while the TUD solution uses regionally distributed sites, resulting in different vertical translation rates and associated velocity patterns. In addition, the TUD analysis applied antenna misalignment corrections, which may have introduced lateral biases further complicating the signal and reducing correction effectiveness.

5 Discussion

This study applied various NTL corrections from two different loading services to reduce the noise and variability in GNSS time series in DML, East Antarctica. The results show that the effectiveness of these corrections depends on the GNSS dataset, its processing strategy, and the station environment. NTAL corrections generally have the most pronounced effect on reducing noise and RMS values, NTOL impacts vary by station, and HYDL mainly shifts the phase of annual amplitudes and reduces them as well as noise in some datasets. Corrections are more effective in datasets with high initial variability and those processed with PPP strategy, such as AY and NGL. Overall, GFZ corrections yielded slightly larger RMS reductions at ABOA and SYOG, while EOST corrections were more effective at VESL.

These findings align with earlier work that has primarily focused on global or Northern Hemisphere GNSS datasets, with Antarctic stations typically included in global studies. Studies such as Niu et al. (2022) found that loading deformation explains

https://doi.org/10.5194/egusphere-2025-5358
Preprint. Discussion started: 7 November 2025

nearly 50 % of the vertical GNSS seasonal displacements, but less than 20 % in the horizontal components. Altamimi et al. (2016) reported improvements in the vertical component at 41 % of global GNSS following NTAL corrections, while Buchta et al. (2025c) observed station-dependent RMS reductions in Antarctica.

Several studies have noted that NTAL corrections help reduce non-seasonal scatter, with particularly strong effects at high latitudes where vertical reductions can exceed 2 mm or 50 % (Buchta et al., 2025c; Gobron et al., 2021; Mémin et al., 2020; Rebischung et al., 2024). While NTOL corrections tend to be more modest and mainly confined to certain coastal regions, HYDL corrections primarily affect annual amplitudes and have minimal impact on non-seasonal scatter. However, both this current study and the one by Jiang et al. (2013) emphasize that the effectiveness of NTL corrections varies substantially depending on the correction models used, the datasets, and the specific station environments. Ejigu & Nordman (2025) show that applying combined NTL (atmospheric, oceanic, and hydrological) corrections greatly improves GNSS time series in northern Europe, reducing vertical WRMS by up to ~58%, halving power-law noise, and lowering trend uncertainties, with hydrological effects introducing annual phase shifts for more accurate geophysical monitoring. In coastal regions, for example, mismodelling of tidal constituents and land-sea mask inconsistencies can introduce additional spurious seasonal signals to the time series (Niu et al., 2022).

On the continental scale, prior findings on NTL correction effectiveness in Antarctica have been mixed. At ABOA, Andrei et al. (2018) found negligible improvements, with vertical trend changes under 0.01 mm/yr and a slight increase in total residual RMS from 5.7 to 6.1 mm. In comparison, this study observed slightly larger differences in trends and RMS values between 3 – 6 mm depending on the dataset, with RMS values generally decreasing after applying the same corrections. Vertical trend estimates also differed (e.g., Andrei et al: 0.79 ± 0.35 mm/yr; AY: 0.44 ± 0.52 mm/yr; OSU: 0.16 ± 0.51 mm/yr; TUD: -0.49 ± 0.67 mm/yr; GR: 0.14 ± 0.39 mm/yr), which may reflect the longer time span used in this study or an increased snow accumulation in recent years introducing elastic loading effectively slowing the post-glacial land uplift (Medley et al., 2018). At SYOG and VESL, the results of this study align well with earlier studies. Mémin et al. (2020) and Gobron et al. (2021) reported vertical WRMS or RMSE reductions of 10 – 20 % at these stations. However, Mémin et al. (2020) noted that NTOL models based on the IB assumption underestimated dynamic pressure effects from the Antarctic Circumpolar Current (ACC), while Gobron et al. (2021) and Koulali et al. (2022) found NTOL improvements limited to 0 – 5 %. In this study, the dynamic ocean model (EOST3) did generally not perform significantly better than those using IB forcing. In addition, the inclusion of NTOL improved performance by only 1 – 3 % in the PPP-processed datasets at ABOA and SYOG. Why ABOA benefits from NTOL to a similar extent as SYOG, but more than VESL, remains unclear, given that both ABOA and VESL are located over 100 km inland from the ice shelf edge, while SYOG is situated on an island. Furthermore, Jiang et al. (2013) also reported negative or positive WRMS changes of up to 20 % depending on the correction model used.

Several studies have further compared the performance of different NTL correction models. For instance, Rebischung et al. (2024) observed that global mean vertical WRMS residuals could be reduced by 19.4 % when applying GFZ corrections and by 20.2 % with EOST models, with NTAL having the largest impact. Similarly, Wu et al. (2020) found that the mean global RMS values decreased by 10.6 % and 15.4 % with GFZ and EOST corrections, respectively. Both studies suggest that EOST

https://doi.org/10.5194/egusphere-2025-5358
Preprint. Discussion started: 7 November 2025

corrections may perform better on a global scale. However, regional variations remain important. In this study, GFZ-based corrections produced marginally better results in the PPP-processed datasets, while EOST models were somewhat more effective for the DD-processed datasets. At station level, Rebischung et al. (2024) and Wu et al. (2020) reported WRMS reductions of approximately 15–30% for GFZ models and 10–20% for EOST models at SYOG and VESL, which is consistent with the results obtained in this study for the PPP-processed datasets. These findings suggest that while EOST models may perform slightly better on a global scale, GFZ corrections can be equally effective in specific Antarctic regions.

NTL corrections have been also shown to impact annual signals. Rebischung et al. (2024) found that global annual amplitudes reduced 56.3 % (GFZ) and 48.4 % (EOST), with HYDL contributing the most to these reductions. Semi-annual amplitudes were reduced by 18.3 % (GFZ) and 15.1 % (EOST), where NTAL had the largest effect. Wu et al. (2020) similarly reported a reduction in annual amplitude of approximately 30 %. They however emphasize that the effect of NTL corrections varies greatly among GNSS stations. In this study, the vertical annual amplitudes generally decreased at each station, with the reductions ranging between approximately 15 % to 70 % depending on the correction model, dataset, and station. As noted by Niu et al. (2023), annual signals exhibit weaker spatial coherence than draconitic signals and often reflect station-specific noise, suggesting that residual seasonal signals post-correction are likely dominated by local environmental effects.

Overall, the results of this study are broadly consistent with previous research, reinforcing the conclusion that the impact of NTL corrections is highly dependent on the choice of model, dataset, and site characteristics. Consistent with earlier findings, correction efficiency is greater at SYOG than at VESL. At the same time, the results also highlight important limitations in current approaches. Antarctica's vast, remote, and environmentally extreme terrain, with sparse infrastructure and logistical constraints, limits spatial coverage and density of geodetic observations. This sparse distribution of observations complicates the detection and validation of localized loading signals and may lead to oversimplified surface load representations (Mémin et al., 2020). Moreover, the coarse spatial resolution of NTL models increases sensitivity to large-scale signals while underrepresenting regional and localized processes, which causes high uncertainties especially in HYDL models (Niu et al., 2022). While different NTAL models typically agree well, significant discrepancies remain between NTOL and HYDL models (Santamaría-Gómez and Mémin, 2015).

In regions like the ACC, NTOL estimates remain uncertain due to limited bottom pressure data and complex wind-driven dynamics (Mémin et al., 2020; Shihora et al., 2022b). Although HYDL corrections performed surprisingly well in this study, current HYDL models are known to be incomplete in Antarctica and may underestimate true deformation, particularly in regions with complex glacial hydrology (Santamaría-Gómez and Mémin, 2015). In addition, unmodelled geophysical processes, such as ongoing ice mass loss, viscoelastic Earth responses to past and present ice and water loading (e.g., GIA), and the presence of groundwater or subglacial aquifers, can substantially influence surface deformation. In particular, temporally correlated glacier mass changes and the viscoelastic rebound of low-viscosity mantle regions may introduce additional unmodelled signals that reduce the accuracy and representativeness of the applied loading corrections.

Residual annual signals in GNSS time series may also reflect monument and site-specific effects not fully captured by loading models. These include thermoelastic and poroelastic deformation of the monument and surrounding ground, as well as

https://doi.org/10.5194/egusphere-2025-5358
Preprint. Discussion started: 7 November 2025

systematic errors such as multipath, antenna phase centre variations under changing snow or ice conditions, mismodelling of tropospheric delays, and sub-daily tidal effects (Rebischung et al., 2024; Niu et al., 2022; He et al., 2017). Draconitic errors and uncorrected atmospheric S1/S2 loading further contribute to unmodelled variability. In addition, discontinuities may arise from equipment changes or maintenance cycles, which are particularly relevant in Antarctica due to long service intervals and harsh conditions. For example, the ABOA receiver was historically exchanged annually between two receivers of the same make and model to retrieve the data and verify receiver performance in Finland. The antenna and receiver were changed 2024 and data was lost in 2006 due to a corrupted memory card and 2021 due to COVID-19 pandemic. On the other hand, SYOG has seen multiple receiver, antenna, and radome changes since 1995, while VESL, though more stable installation, upgraded its receiver in 2008 and relies on an internal oscillator less precise than SYOG's caesium standard (Buchta et al., 2025a; Finnish Meteorological Institute, 2024; Scheinert et al., 2023). Moreover, snow accumulation on GNSS antennas or intrusion through drainage holes can lead to outliers and time series discontinuities, with vertical displacements of approximately 3 – 5 mm (He et al., 2017; Larson, 2013; Koulali and Clarke, 2020; Dong et al., 2002). These effects add noise that may obscure subtle geophysical signals.

This study also showed significant differences in correction effectiveness across different GNSS datasets, emphasizing the influence of processing strategy. The independently processed AY dataset demonstrated larger RMS and noise reductions than external solutions, particularly at ABOA and SYOG, suggesting that correction performance is partially influenced by baseline noise levels and processing choices. While the tested NTL corrections proved reasonably effective, further improvements are likely through the development of models tailored to the Antarctic environment. Existing global models may fail to fully capture regional hydrological and oceanic processes, limiting their accuracy at certain stations. Increasing the spatial and temporal resolution of NTL models, developing region-specific corrections, and independently computing loading displacements could all improve displacement estimates further. Integrating complementary datasets, such as satellite altimetry, gravimetry, or InSAR, could help overcome data gaps and support the development of more accurate, site-specific NTL corrections. For now, correcting for NTL remains a major challenge for the sparce and unevenly distributed GNSS network in Antarctica.

6 Conclusion

This study evaluated the impact of NTL corrections on vertical GNSS time series across three Antarctic stations, ABOA, SYOG, and VESL, using five distinct datasets (AY, NGL, GR, OSU, and TUD), and 11 different correction model combinations. The results show that NTL corrections can significantly improve time series quality by reducing RMS, noise, and seasonal amplitudes, particularly in datasets with high initial variability such as AY and NGL. Several central findings emerge from the analysis.

First, the GNSS processing strategy plays a significant role in determining correction effectiveness. The PPP-processed datasets, AY and NGL, consistently responded more positively to loading corrections than the network-based DD solutions

https://doi.org/10.5194/egusphere-2025-5358
Preprint. Discussion started: 7 November 2025

(OSU and TUD) or the combined solution (GR). In PPP datasets, vertical RMS was frequently reduced by more than 20 %, while the already NTAL-corrected GR dataset showed limited sensitivity to further adjustments. In several cases, additional corrections introduced new variability by increased noise levels and RMS.

Second, the relative contributions of NTAL, NTOL, and HYDL components varied by station and dataset. NTAL alone typically yielded the most consistent reductions in RMS, noise, and seasonal amplitudes. The combined application of NTOL and HYDL improved performance only in the PPP-processed datasets. Applying the same combinations to DD-processed or combined datasets often introduced additional variability. The inclusion of NTOL had limited impact at VESL but produced more substantial improvements at ABOA and SYOG. HYDL effects were more variable, depending on both dataset and station. While some combinations (e.g., GFZ3 applied to AY or NGL at ABOA) led to improvements, other applications (e.g., GFZ5 applied to GR) increased RMS, noise, and seasonal amplitudes.

Third, the choice of NTL model had only a limited effect on correction performance. Differences between the models by the different providers were minimal. GFZ-based corrections tended to outperform EOST models in reducing vertical RMS, noise, and seasonal amplitudes in the PPP-processed datasets at ABOA and SYOG, with GFZ3 consistently emerging as one of the most effective models. In contrast, EOST corrections performed better at VESL, where GFZ models were generally less effective. These differences suggest that both environmental conditions and model parameterisation influence correction outcomes. Further research is needed to better understand these regional differences and to refine model inputs so that NTL corrections can be more reliably applied across the Antarctic continent.

Finally, this study shows that the choice of GNSS processing strategy and NTL model choices can affect the estimated vertical trends, in some cases even altering their direction. This has critical implications for GIA research, where GNSS is used to validate geophysical models or construct empirical ones, emphasizing the need for careful consideration of both processing methods and correction strategies. Since ready-processed GNSS datasets and open global NTL models include many parameters that influence results but cannot be fine-tuned by the user, future work will focus on performing both the GNSS processing and NTL model computations in-house to assess whether the findings are robust and consistent.

finding

Appendix A: Hector time series analysis

Table A1: Estimated trends, seasonal amplitudes, and noise parameters from Hector analysis with different corrections at ABOA, SYOG, and VESL stations.

Station	*Dataset*	*Correction*	*Trend (mm/yr)*	*Trend σ (mm/yr)*	*Annual Amp (mm)*	*Annual Amp σ (mm)*	*Semi-Annual Amp (mm)*	*Semi-Annual Amp σ (mm)*	σ_{PL} $\left(mm/yr^{\hat{\kappa}/4}\right)$	σ_{WN} *(mm)*	$\hat{\kappa}$
ABOA	AY	Original	0.44	0.52	2.46	0.48	1.15	0.34	16.43	0.46	-0.96
ABOA	AY	EOST1	0.53	0.36	1.49	0.31	1.08	0.22	10.14	2.46	-1.01
ABOA	AY	EOST2	0.45	0.25	1.41	0.26	1.10	0.20	10.17	0.30	-0.72
ABOA	AY	GFZ1	0.45	0.26	1.35	0.27	1.03	0.21	10.38	0.36	-0.73

https://doi.org/10.5194/egusphere-2025-5358
Preprint. Discussion started: 7 November 2025

ABOA	AY	EOST3	0.45	0.28	1.36	0.27	1.05	0.20	9.91	1.88	-0.85
ABOA	AY	EOST4	0.44	0.26	1.25	0.27	1.11	0.20	10.25	0.74	-0.75
ABOA	AY	EOST5	0.43	0.20	1.17	0.22	1.13	0.17	8.71	1.26	-0.68
ABOA	AY	GFZ2	0.50	0.23	1.25	0.24	1.11	0.19	9.32	1.02	-0.71
ABOA	AY	GFZ3	0.37	0.11	0.55	0.14	1.39	0.12	6.41	0.72	-0.42
ABOA	OSU	Original	0.16	0.51	2.26	0.42	1.23	0.28	12.73	1.04	-1.17
ABOA	OSU	EOST1	0.18	0.11	1.79	0.13	0.86	0.11	5.60	0.48	-0.56
ABOA	OSU	EOST2	0.17	0.51	1.76	0.42	0.91	0.28	12.97	0.01	-1.16
ABOA	OSU	GFZ1	0.18	0.12	1.71	0.14	0.84	0.11	5.81	0.31	-0.60
ABOA	OSU	EOST3	0.15	0.41	1.87	0.35	0.84	0.24	11.31	0.33	-1.08
ABOA	OSU	EOST4	0.16	0.17	1.77	0.18	0.85	0.14	6.94	0.02	-0.71
ABOA	OSU	EOST5	0.17	0.29	1.71	0.27	0.89	0.19	9.14	0.61	-0.94
ABOA	OSU	GFZ2	0.29	0.48	1.94	0.40	0.90	0.26	12.25	0.68	-1.16
ABOA	OSU	GFZ3	0.23	0.28	0.38	0.19	1.10	0.19	9.05	0.00	-0.91
ABOA	TUD	Original	-0.49	0.67	1.09	0.46	0.70	0.31	16.08	1.33	-1.02
ABOA	TUD	EOST1	0.16	0.29	1.32	0.25	0.93	0.19	9.12	1.59	-0.70
ABOA	TUD	EOST2	-0.12	0.42	1.24	0.34	0.97	0.25	11.71	1.18	-0.84
ABOA	TUD	GFZ1	-0.24	0.48	1.31	0.38	0.90	0.27	12.65	1.34	-0.91
ABOA	TUD	EOST3	0.42	0.19	1.72	0.18	0.94	0.15	7.65	0.87	-0.49
ABOA	TUD	EOST4	0.54	0.14	1.68	0.15	0.97	0.13	6.32	1.54	-0.38
ABOA	TUD	EOST5	0.48	0.18	1.64	0.17	1.00	0.15	7.34	0.90	-0.46
ABOA	TUD	GFZ2	-0.18	0.52	2.06	0.41	1.04	0.29	13.72	0.65	-0.91
ABOA	TUD	GFZ3	0.26	0.21	1.29	0.20	1.26	0.17	8.16	0.85	-0.54
ABOA	GR	Original	0.14	0.39	2.60	0.31	0.81	0.22	9.92	0.55	-0.97
ABOA	GR	EOST6	0.14	0.39	3.05	0.31	0.86	0.22	10.06	0.17	-0.96
ABOA	GR	GFZ4	0.22	0.46	3.43	0.36	0.93	0.24	10.95	0.77	-1.04
ABOA	GR	GFZ5	0.03	0.49	2.60	0.38	1.21	0.25	11.32	0.87	-1.08
SYOG	AY	Original	1.10	0.23	2.81	0.33	0.99	0.25	12.97	0.00	-0.80
SYOG	AY	EOST1	1.01	0.14	1.54	0.20	0.61	0.15	7.80	2.33	-0.76
SYOG	AY	EOST2	1.02	0.14	1.48	0.20	0.64	0.15	7.82	2.35	-0.76
SYOG	AY	GFZ1	1.01	0.13	1.39	0.20	0.63	0.15	7.79	2.30	-0.74
SYOG	AY	EOST3	1.03	0.14	1.34	0.20	0.65	0.15	7.43	2.57	-0.83
SYOG	AY	EOST4	1.05	0.14	1.32	0.20	0.59	0.15	7.48	2.54	-0.81
SYOG	AY	EOST5	1.07	0.14	1.25	0.20	0.61	0.15	7.47	2.56	-0.82
SYOG	AY	GFZ2	1.12	0.15	0.98	0.19	0.66	0.15	7.19	2.65	-0.87
SYOG	AY	GFZ3	1.14	0.14	1.47	0.19	0.96	0.15	7.12	2.66	-0.86
SYOG	NGL	Original	0.83	0.28	2.52	0.38	1.10	0.27	14.24	0.00	-0.87
SYOG	NGL	EOST1	0.80	0.19	1.95	0.25	0.57	0.18	9.24	2.32	-0.90
SYOG	NGL	EOST2	0.82	0.19	1.88	0.25	0.59	0.18	9.23	2.34	-0.90
SYOG	NGL	GFZ1	0.81	0.19	1.90	0.25	0.57	0.18	9.22	2.30	-0.88

https://doi.org/10.5194/egusphere-2025-5358
Preprint. Discussion started: 7 November 2025

SYOG	NGL	EOST3	0.82	0.20	2.10	0.25	0.58	0.18	9.00	2.51	-0.96
SYOG	NGL	EOST4	0.85	0.20	2.00	0.25	0.53	0.17	8.93	2.51	-0.96
SYOG	NGL	EOST5	0.87	0.20	1.94	0.25	0.55	0.18	8.94	2.52	-0.96
SYOG	NGL	GFZ2	0.91	0.21	2.05	0.25	0.60	0.18	8.78	2.57	-0.99
SYOG	NGL	GFZ3	0.92	0.20	0.51	0.22	0.87	0.18	8.74	2.57	-0.98
SYOG	OSU	Original	0.81	0.22	2.69	0.28	0.85	0.20	10.40	0.00	-0.93
SYOG	OSU	EOST1	0.75	0.20	1.39	0.25	0.46	0.17	8.95	0.94	-0.96
SYOG	OSU	EOST2	0.76	0.20	1.33	0.25	0.49	0.17	8.98	0.94	-0.96
SYOG	OSU	GFZ1	0.75	0.19	1.25	0.25	0.49	0.17	9.02	0.84	-0.94
SYOG	OSU	EOST3	0.74	0.19	1.21	0.25	0.51	0.17	9.30	0.00	-0.90
SYOG	OSU	EOST4	0.78	0.20	1.18	0.26	0.45	0.17	9.36	0.77	-0.96
SYOG	OSU	EOST5	0.79	0.21	1.11	0.26	0.48	0.18	9.40	0.77	-0.96
SYOG	OSU	GFZ2	0.81	0.21	0.90	0.27	0.54	0.19	9.95	0.00	-0.94
SYOG	OSU	GFZ3	0.81	0.21	1.37	0.27	0.81	0.19	9.93	0.00	-0.94
SYOG	TUD	Original	0.75	0.30	1.33	0.36	0.55	0.24	12.45	1.44	-0.98
SYOG	TUD	EOST1	0.71	0.37	1.50	0.36	0.64	0.24	11.32	2.18	-1.15
SYOG	TUD	EOST2	0.72	0.37	1.47	0.37	0.66	0.24	11.37	2.19	-1.16
SYOG	TUD	GFZ1	0.72	0.36	1.59	0.36	0.69	0.24	11.40	2.16	-1.13
SYOG	TUD	EOST3	0.71	0.35	1.93	0.37	0.75	0.24	11.47	2.08	-1.12
SYOG	TUD	EOST4	0.75	0.38	1.81	0.38	0.68	0.24	11.57	2.18	-1.16
SYOG	TUD	EOST5	0.76	0.39	1.79	0.38	0.70	0.24	11.62	2.19	-1.17
SYOG	TUD	GFZ2	0.78	0.36	2.25	0.38	0.76	0.25	11.94	2.04	-1.12
SYOG	TUD	GFZ3	0.72	0.35	1.09	0.36	0.97	0.25	11.83	2.02	-1.10
SYOG	GR	Original	0.53	0.16	2.13	0.21	1.08	0.16	7.66	0.81	-0.87
SYOG	GR	EOST6	0.56	0.17	2.54	0.23	1.11	0.17	8.38	0.27	-0.86
SYOG	GR	GFZ4	0.59	0.21	2.96	0.27	1.16	0.19	9.46	0.00	-0.91
SYOG	GR	GFZ5	0.55	0.21	2.13	0.27	1.39	0.19	9.46	0.00	-0.91
VESL	AY	Original	0.66	0.44	4.80	0.58	1.27	0.39	18.82	0.00	-1.07
VESL	AY	EOST1	0.58	0.24	3.15	0.35	0.95	0.25	12.09	1.60	-0.96
VESL	AY	EOST2	0.59	0.24	3.13	0.35	0.97	0.25	12.06	1.61	-0.96
VESL	AY	GFZ1	0.61	0.24	3.11	0.36	0.95	0.26	12.38	1.51	-0.97
VESL	AY	EOST3	0.58	0.26	2.80	0.36	1.00	0.25	11.74	1.87	-1.03
VESL	AY	EOST4	0.59	0.24	2.68	0.35	0.97	0.25	11.79	1.79	-0.99
VESL	AY	EOST5	0.60	0.24	2.66	0.35	0.99	0.25	11.76	1.79	-0.99
VESL	AY	GFZ2	0.65	0.25	2.34	0.35	1.01	0.25	11.54	1.91	-1.02
VESL	AY	GFZ3	0.61	0.25	2.53	0.34	1.35	0.24	11.33	1.95	-1.03
VESL	NGL	Original	0.33	0.47	3.83	0.59	1.19	0.39	18.91	0.00	-1.10
VESL	NGL	EOST1	0.27	0.21	2.67	0.33	0.68	0.23	11.52	1.25	-0.92
VESL	NGL	EOST2	0.28	0.21	2.62	0.33	0.70	0.23	11.48	1.30	-0.92
VESL	NGL	GFZ1	0.31	0.22	2.62	0.34	0.71	0.24	11.93	1.09	-0.93

https://doi.org/10.5194/egusphere-2025-5358
Preprint. Discussion started: 7 November 2025

VESL	NGL	EOST3	0.29	0.23	2.53	0.32	0.66	0.22	10.90	1.70	-0.99
VESL	NGL	EOST4	0.29	0.21	2.37	0.32	0.65	0.22	11.17	1.53	-0.95
VESL	NGL	GFZ2	0.36	0.22	2.24	0.32	0.67	0.22	10.93	1.69	-0.98
VESL	NGL	GFZ3	0.31	0.21	1.36	0.31	0.97	0.23	10.88	1.63	-0.96
VESL	OSU	Original	0.21	0.34	3.75	0.42	1.26	0.29	13.80	0.00	-1.09
VESL	OSU	EOST1	0.14	0.28	2.62	0.37	0.62	0.24	12.27	0.00	-1.06
VESL	OSU	EOST2	0.16	0.28	2.56	0.37	0.63	0.24	12.29	0.00	-1.06
VESL	OSU	GFZ1	0.18	0.26	2.54	0.34	0.66	0.23	11.49	0.58	-1.06
VESL	OSU	EOST3	0.15	0.29	2.43	0.36	0.57	0.23	11.89	0.43	-1.09
VESL	OSU	EOST4	0.15	0.31	2.33	0.39	0.56	0.24	12.89	0.00	-1.08
VESL	OSU	EOST5	0.17	0.31	2.25	0.39	0.57	0.24	12.84	0.00	-1.09
VESL	OSU	GFZ2	0.22	0.31	2.16	0.38	0.60	0.24	12.74	0.00	-1.09
VESL	OSU	GFZ3	0.18	0.28	1.36	0.36	0.80	0.25	12.10	0.00	-1.06
VESL	TUD	Original	0.11	0.43	2.33	0.54	0.87	0.35	16.98	1.64	-1.05
VESL	TUD	EOST1	0.00	0.41	1.32	0.46	0.55	0.27	14.51	2.23	-1.11
VESL	TUD	EOST2	0.01	0.41	1.24	0.45	0.56	0.27	14.41	2.25	-1.11
VESL	TUD	GFZ1	0.04	0.44	1.28	0.46	0.55	0.27	14.40	2.36	-1.15
VESL	TUD	EOST3	0.01	0.44	1.36	0.46	0.58	0.28	14.34	2.33	-1.16
VESL	TUD	EOST4	0.02	0.41	1.22	0.45	0.57	0.27	14.57	2.21	-1.11
VESL	TUD	EOST5	0.03	0.41	1.14	0.44	0.57	0.27	14.48	2.21	-1.11
VESL	TUD	GFZ2	0.07	0.41	1.30	0.46	0.59	0.28	14.43	2.24	-1.12
VESL	TUD	GFZ3	0.01	0.43	0.66	0.34	0.92	0.32	14.65	2.28	-1.14
VESL	GR	Original	0.10	0.27	1.92	0.32	0.57	0.21	9.95	1.10	-1.09
VESL	GR	EOST6	0.11	0.27	2.27	0.33	0.64	0.22	10.28	0.99	-1.08
VESL	GR	GFZ4	0.13	0.25	2.61	0.33	0.69	0.23	10.81	0.10	-1.01
VESL	GR	GFZ5	0.05	0.25	1.78	0.33	1.05	0.23	10.88	0.00	-1.01

585

Appendix B: RMS evaluation

Table B1: Percentage change in RMS values after applying different loading corrections at the ABOA, SYOG, and VESL stations. Negative values indicate an increase in RMS, while positive values indicate a reduction.

Station	*Dataset*	*Correction*	*RMS (mm)*	*RMS change (%)*
ABOA	AY	Original	5.61	0.00
ABOA	AY	EOST1	4.54	18.99
ABOA	AY	EOST2	4.39	21.69
ABOA	AY	GFZ1	4.47	20.36
ABOA	AY	EOST3	4.43	21.02
ABOA	AY	EOST4	4.38	21.89

https://doi.org/10.5194/egusphere-2025-5358
Preprint. Discussion started: 7 November 2025

ABOA	AY	EOST5	4.34	22.58
ABOA	AY	GFZ2	4.30	23.28
ABOA	AY	GFZ3	4.15	26.04
ABOA	OSU	Original	3.75	0.00
ABOA	OSU	EOST1	3.47	7.33
ABOA	OSU	EOST2	3.63	3.11
ABOA	OSU	GFZ1	3.35	10.54
ABOA	OSU	EOST3	3.61	3.62
ABOA	OSU	EOST4	3.60	3.78
ABOA	OSU	EOST5	3.70	1.30
ABOA	OSU	GFZ2	3.78	-1.05
ABOA	OSU	GFZ3	3.60	3.77
ABOA	TUD	Original	5.69	0.00
ABOA	TUD	EOST1	4.84	14.84
ABOA	TUD	EOST2	4.94	13.18
ABOA	TUD	GFZ1	5.01	11.90
ABOA	TUD	EOST3	4.84	14.98
ABOA	TUD	EOST4	4.81	15.47
ABOA	TUD	EOST5	4.81	15.37
ABOA	TUD	GFZ2	5.09	10.55
ABOA	TUD	GFZ3	4.90	13.92
ABOA	GR	Original	3.34	0.00
ABOA	GR	EOST6	3.38	-1.32
ABOA	GR	GFZ4	3.49	-4.54
ABOA	GR	GFZ5	3.50	-4.89
SYOG	AY	Original	4.97	0.00
SYOG	AY	EOST1	3.95	20.53
SYOG	AY	EOST2	3.96	20.32
SYOG	AY	GFZ1	3.95	20.41
SYOG	AY	EOST3	3.87	22.01
SYOG	AY	EOST4	3.88	21.84
SYOG	AY	EOST5	3.89	21.68
SYOG	AY	GFZ2	3.81	23.21
SYOG	AY	GFZ3	3.82	23.18
SYOG	NGL	Original	5.20	0.00
SYOG	NGL	EOST1	4.18	19.69
SYOG	NGL	EOST2	4.18	19.70

https://doi.org/10.5194/egusphere-2025-5358
Preprint. Discussion started: 7 November 2025

SYOG	NGL	GFZ1	4.18	19.61
SYOG	NGL	EOST3	4.16	20.09
SYOG	NGL	EOST4	4.13	20.58
SYOG	NGL	EOST5	4.14	20.47
SYOG	NGL	GFZ2	4.09	21.32
SYOG	NGL	GFZ3	4.10	21.19
SYOG	OSU	Original	3.68	0.00
SYOG	OSU	EOST1	3.33	9.50
SYOG	OSU	EOST2	3.34	9.19
SYOG	OSU	GFZ1	3.35	8.99
SYOG	OSU	EOST3	3.41	7.21
SYOG	OSU	EOST4	3.41	7.29
SYOG	OSU	EOST5	3.42	7.02
SYOG	OSU	GFZ2	3.53	3.98
SYOG	OSU	GFZ3	3.53	4.19
SYOG	TUD	Original	4.71	0.00
SYOG	TUD	EOST1	4.61	2.00
SYOG	TUD	EOST2	4.63	1.67
SYOG	TUD	GFZ1	4.55	3.30
SYOG	TUD	EOST3	4.64	1.44
SYOG	TUD	EOST4	4.70	0.21
SYOG	TUD	EOST5	4.71	0.02
SYOG	TUD	GFZ2	4.71	-0.13
SYOG	TUD	GFZ3	4.65	1.19
SYOG	GR	Original	3.05	0.00
SYOG	GR	EOST6	3.21	-5.08
SYOG	GR	GFZ4	3.44	-12.63
SYOG	GR	GFZ5	3.44	-12.70
VESL	AY	Original	7.03	0.00
VESL	AY	EOST1	6.05	13.99
VESL	AY	EOST2	6.05	13.91
VESL	AY	GFZ1	6.12	12.91
VESL	AY	EOST3	6.00	14.62
VESL	AY	EOST4	6.01	14.45
VESL	AY	EOST5	6.02	14.37
VESL	AY	GFZ2	6.03	14.24
VESL	AY	GFZ3	5.98	14.94

https://doi.org/10.5194/egusphere-2025-5358
Preprint. Discussion started: 7 November 2025

VESL	NGL	Original	7.14	0.00
VESL	NGL	EOST1	6.01	15.91
VESL	NGL	EOST2	6.02	15.78
VESL	NGL	GFZ1	6.15	13.93
VESL	NGL	EOST3	5.96	16.58
VESL	NGL	EOST4	5.98	16.31
VESL	NGL	EOST5	5.97	16.50
VESL	NGL	GFZ2	6.06	15.22
VESL	NGL	GFZ3	6.04	15.45
VESL	OSU	Original	5.53	0.00
VESL	OSU	EOST1	5.43	1.74
VESL	OSU	EOST2	5.45	1.46
VESL	OSU	GFZ1	5.38	2.57
VESL	OSU	EOST3	5.35	3.10
VESL	OSU	EOST4	5.49	0.66
VESL	OSU	EOST5	5.51	0.36
VESL	OSU	GFZ2	5.50	0.50
VESL	OSU	GFZ3	5.39	2.54
VESL	TUD	Original	6.90	0.00
VESL	TUD	EOST1	6.42	6.94
VESL	TUD	EOST2	6.41	7.10
VESL	TUD	GFZ1	6.50	5.74
VESL	TUD	EOST3	6.41	7.12
VESL	TUD	EOST4	6.37	7.65
VESL	TUD	EOST5	6.36	7.79
VESL	TUD	GFZ2	6.40	7.24
VESL	TUD	GFZ3	6.52	5.47
VESL	GR	Original	5.21	0.00
VESL	GR	EOST6	5.19	0.41
VESL	GR	GFZ4	5.18	0.51
VESL	GR	GFZ5	5.30	-1.66

590

https://doi.org/10.5194/egusphere-2025-5358
Preprint. Discussion started: 7 November 2025

Data and code availability

Data are available through various open repositories. NGL data can be accessed at https://geodesy.unr.edu/NGLStationPages/stations/, and GR data at https://doi.pangaea.de/10.1594/PANGAEA.967516. The AY solution can be provided by the corresponding author upon request. Code is available at the following GitHub repository in two Jupyter notebooks: https://github.com/ainoschulz/Antarctica_NTL

Author contribution

AS: data collection, formal analysis, writing – original draft, writing – review & editing, visualization, data curation; YE: data collection, GNSS processing (AY dataset), writing – review & editing; JN: data collection, writing – review & editing; MN: original research idea and conceptualization, funding acquisition, writing – review & editing, supervision

Competing interests

The authors declare that they have no conflict of interest.

Acknowledgements

The calculations were performed on HPC resources of the Aalto University School of Science "Science-IT" project. We are grateful for Eric Buchta (TUD) and Eric Kendrick (OSU) for providing us two of the four composite solutions of the GR dataset.
PolarToolkit v0.8.1 (Tankersley, 2024) was used to generate the map in Figure 1.
AI-tools were used to help with language and grammar.

Financial support

This research was funded by the Väisälä project grant of the Finnish Academy of Science and Letters and the Research Council of Finland (decision number 364868).

References

Altamimi, Z., Rebischung, P., Métivier, L., and Collilieux, X.: ITRF2014: A new release of the International Terrestrial Reference Frame modeling nonlinear station motions, Journal of Geophysical Research: Solid Earth, 121, 6109–6131, 10.1002/2016JB013098, 2016.

https://doi.org/10.5194/egusphere-2025-5358
Preprint. Discussion started: 7 November 2025

Altamimi, Z., Rebischung, P., Collilieux, X., Métivier, L., and Chanard, K.: ITRF2020: an augmented reference frame refining the modeling of nonlinear station motions, Journal of Geodesy, 97, 47, 10.1007/s00190-023-01738-w, 2023.

Andrei, C.-O., Lahtinen, S., Nordman, M., Näränen, J., Koivula, H., Poutanen, M., and Hyyppä, J.: GPS Time Series Analysis from Aboa the Finnish Antarctic Research Station, Remote Sensing, 10, 1937, 10.3390/rs10121937, 2018.

Bevis, M., Bedford, J., and Caccamise II, D. J.: The Art and Science of Trajectory Modelling, in: Geodetic Time Series Analysis in Earth Sciences, edited by: Montillet, J.-P., and Bos, M. S., Springer International Publishing, Cham, 1–27, 10.1007/978-3-030-21718-1_1, 2020.

Blewitt, G., Hammond, W. C., and Kreemer, C.: Harnessing the GPS data explosion for interdisciplinary science, Eos, 99, 10.1029/2018EO104623, 2018.

Bos, M. S., Bastos, L., and Fernandes, R. M. S.: The influence of seasonal signals on the estimation of the tectonic motion in short continuous GPS time-series, Journal of Geodynamics, 49, 205–209, 10.1016/j.jog.2009.10.005, 2010.

Bos, M. S., Fernandes, R. M. S., Williams, S. D. P., and Bastos, L.: Fast error analysis of continuous GNSS observations with missing data, Journal of Geodesy, 87, 351–360, 10.1007/s00190-012-0605-0, 2013.

Boy, J.-P.: Contribution of GGFC to ITRF2020, 2021.

Buchta, E., Scheinert, M., King, M., Wilson, T., Clarke, P. J., Gómez, D., Kendrick, E., Knöfel, C., and Koulali, A.: Station information for GPS stations on bedrock for Antarctica and the sub Antarctic sector, 1995-2021, PANGAEA [dataset], 10.1594/PANGAEA.967532, 2025a.

Buchta, E., Scheinert, M., King, M., Wilson, T., Clarke, P. J., Gómez, D., Kendrick, E., Knöfel, C., and Koulali, A.: Daily coordinate time series for GPS stations on bedrock for Antarctica and the sub Antarctic sector, 1995-2021, PANGAEA [dataset], 10.1594/PANGAEA.967516, 2025b.

Buchta, E., Scheinert, M., King, M. A., Wilson, T., Koulali, A., Clarke, P. J., Gómez, D., Kendrick, E., Knöfel, C., and Busch, P.: Advancing geodynamic research in Antarctica: reprocessing GNSS data to infer consistent coordinate time series (GIANT-REGAIN), Earth Syst. Sci. Data, 17, 1761–1780, 10.5194/essd-17-1761-2025, 2025c.

Dill, R. and Dobslaw, H.: Numerical simulations of global-scale high-resolution hydrological crustal deformations, Journal of Geophysical Research: Solid Earth, 118, 5008–5017, 10.1002/jgrb.50353, 2013.

Dill, R., Dobslaw, H., and Thomas, M.: ESMGFZ Products for Earth Rotation Prediction, Artificial Satellites, 57, 254–261, 10.2478/arsa-2022-0022, 2022.

Dong, D., Fang, P., Bock, Y., Cheng, M. K., and Miyazaki, S.: Anatomy of apparent seasonal variations from GPS-derived site position time series, Journal of Geophysical Research: Solid Earth, 107, ETG 9–1–ETG 9–16, 10.1029/2001JB000573, 2002.

Dziewonski, A. M. and Anderson, D. L.: Preliminary reference Earth model, Physics of the Earth and Planetary Interiors, 25, 297–356, 10.1016/0031-9201(81)90046-7, 1981.

Ejigu, Y. G. and Nordman, M.: Improving GNSS data accuracy: Implementing Non-tidal Corrections at the Observation-level in GNSS data, GPS Solutions, 29, 159, 10.1007/s10291-025-01921-w, 2025.

https://doi.org/10.5194/egusphere-2025-5358
Preprint. Discussion started: 7 November 2025

Ejigu, Y. G., Boy, J.-P., Raja-Halli, A., Khorrami, F., Naranen, J., and Nordman, M.: Analyzing the 3D Deformation Induced by Non-tidal Loading in GNSS Time Series in Finland, in: International Association of Geodesy Symposia, Springer Berlin Heidelberg, Berlin, Heidelberg, 1–8, 10.1007/1345_2024_259, 2024.

Farrell, W. E.: Deformation of the Earth by surface loads, Reviews of Geophysics, 10, 761–797, 10.1029/RG010i003p00761, 1972.

Finnish Meteorological Institute: FINNARP Field Operations 2023–24, Helsinki, 2024.

Gelaro, R., McCarty, W., Suárez, M. J., Todling, R., Molod, A., Takacs, L., Randles, C. A., Darmenov, A., Bosilovich, M. G., Reichle, R., Wargan, K., Coy, L., Cullather, R., Draper, C., Akella, S., Buchard, V., Conaty, A., da Silva, A. M., Gu, W., Kim, G.-K., Koster, R., Lucchesi, R., Merkova, D., Nielsen, J. E., Partyka, G., Pawson, S., Putman, W., Rienecker, M., Schubert, S. D., Sienkiewicz, M., and Zhao, B.: The Modern-Era Retrospective Analysis for Research and Applications, Version 2 (MERRA-2), Journal of Climate, 30, 5419–5454, 10.1175/JCLI-D-16-0758.1, 2017.

Glomsda, M., Seitz, M., Bloßfeld, M., and Seitz, F.: Effects of non-tidal loading applied in VLBI-only terrestrial reference frames, Journal of Geodesy, 97, 76, 10.1007/s00190-023-01766-6, 2023.

Glomsda, M., Bloßfeld, M., Seitz, M., Angermann, D., and Seitz, F.: Comparison of non-tidal loading data for application in a secular terrestrial reference frame, Earth, Planets and Space, 74, 87, 10.1186/s40623-022-01634-1, 2022.

Gobron, K., Rebischung, P., Chanard, K., and Altamimi, Z.: Anatomy of the spatiotemporally correlated noise in GNSS station position time series, Journal of Geodesy, 98, 34, 10.1007/s00190-024-01848-z, 2024.

Gobron, K., Rebischung, P., Van Camp, M., Demoulin, A., and de Viron, O.: Influence of Aperiodic Non-Tidal Atmospheric and Oceanic Loading Deformations on the Stochastic Properties of Global GNSS Vertical Land Motion Time Series, Journal of Geophysical Research: Solid Earth, 126, e2021JB022370, 10.1029/2021JB022370, 2021.

He, X., Bos, M. S., Montillet, J. P., and Fernandes, R. M. S.: Investigation of the noise properties at low frequencies in long GNSS time series, Journal of Geodesy, 93, 1271–1282, 10.1007/s00190-019-01244-y, 2019.

He, X., Montillet, J.-P., Fernandes, R., Bos, M., Yu, K., Hua, X., and Jiang, W.: Review of current GPS methodologies for producing accurate time series and their error sources, Journal of Geodynamics, 106, 12–29, 10.1016/j.jog.2017.01.004, 2017.

Hohensinn, R., Ruttner, P., and Bock, Y.: Sensitivity of GNSS to vertical land motion over Europe: effects of geophysical loadings and common-mode errors, Journal of Geodesy, 98, 68, 10.1007/s00190-024-01856-z, 2024.

Jiang, W., Li, Z., van Dam, T., and Ding, W.: Comparative analysis of different environmental loading methods and their impacts on the GPS height time series, Journal of Geodesy, 87, 687–703, 10.1007/s00190-013-0642-3, 2013.

Jungclaus, J. H., Fischer, N., Haak, H., Lohmann, K., Marotzke, J., Matei, D., Mikolajewicz, U., Notz, D., and von Storch, J. S.: Characteristics of the ocean simulations in the Max Planck Institute Ocean Model (MPIOM) the ocean component of the MPI-Earth system model, Journal of Advances in Modeling Earth Systems, 5, 422–446, 10.1002/jame.20023, 2013.

Kennett, B. L. N., Engdahl, E. R., and Buland, R.: Constraints on seismic velocities in the Earth from traveltimes, Geophysical Journal International, 122, 108–124, 10.1111/j.1365-246X.1995.tb03540.x, 1995.

Khorrami, F., Ejigu, Y. G., Näränen, J., Raja-Halli, A., and Nordman, M.: Exploring Non-tidal Atmospheric Loading Deformation Correction in GNSS Time Series Analysis Using GAMIT/GLOBK Software, in, Springer Berlin Heidelberg, Berlin, Heidelberg, 1–15, 10.1007/1345_2024_272, 2024.

https://doi.org/10.5194/egusphere-2025-5358
Preprint. Discussion started: 7 November 2025

Klos, A., Dobslaw, H., Dill, R., and Bogusz, J.: Identifying the sensitivity of GPS to non-tidal loadings at various time resolutions: examining vertical displacements from continental Eurasia, GPS Solutions, 25, 89, 10.1007/s10291-021-01135-w, 2021.

Klos, A., Olivares, G., Teferle, F. N., Hunegnaw, A., and Bogusz, J.: On the combined effect of periodic signals and colored noise on velocity uncertainties, GPS Solutions, 22, 1, 10.1007/s10291-017-0674-x, 2017.

Kotsakis, C. and Chatzinikos, M.: Terrestrial reference frames and their internal accuracy at coordinate system level, Journal of Geodesy, 97, 107, 10.1007/s00190-023-01801-6, 2023.

Koulali, A. and Clarke, P. J.: Effect of antenna snow intrusion on vertical GPS position time series in Antarctica, Journal of Geodesy, 94, 101, 10.1007/s00190-020-01403-6, 2020.

Koulali, A., Whitehouse, P. L., Clarke, P. J., van den Broeke, M. R., Nield, G. A., King, M. A., Bentley, M. J., Wouters, B., and Wilson, T.: GPS-Observed Elastic Deformation Due to Surface Mass Balance Variability in the Southern Antarctic Peninsula, Geophysical Research Letters, 49, e2021GL097109, 10.1029/2021GL097109, 2022.

Larson, K. M.: A methodology to eliminate snow- and ice-contaminated solutions from GPS coordinate time series, Journal of Geophysical Research: Solid Earth, 118, 4503–4510, 10.1002/jgrb.50307, 2013.

Li, Z., Jiang, W., van Dam, T., Zou, X., Chen, Q., and Chen, H.: A Review on Modeling Environmental Loading Effects and Their Contributions to Nonlinear Variations of Global Navigation Satellite System Coordinate Time Series, Engineering, 47, 26–37, 10.1016/j.eng.2024.09.001, 2025.

Liu, B., King, M., and Dai, W.: Common mode error in Antarctic GPS coordinate time-series on its effect on bedrock-uplift estimates, Geophysical Journal International, 214, 1652–1664, 10.1093/gji/ggy217, 2018.

Liu, J., Chen, J., Liu, P., Tan, W., Dong, D., and Qu, W.: Comparison and Assessment of Three ITRS Realizations, Remote Sensing, 13, 2304, 10.3390/rs13122304, 2021.

Männel, B., Dobslaw, H., Dill, R., Glaser, S., Balidakis, K., Thomas, M., and Schuh, H.: Correcting surface loading at the observation level: impact on global GNSS and VLBI station networks, Journal of Geodesy, 93, 2003–2017, 10.1007/s00190-019-01298-y, 2019.

Martens, H. R., Argus, D. F., Norberg, C., Blewitt, G., Herring, T. A., Moore, A. W., Hammond, W. C., and Kreemer, C.: Atmospheric pressure loading in GPS positions: dependency on GPS processing methods and effect on assessment of seasonal deformation in the contiguous USA and Alaska, Journal of Geodesy, 94, 115, 10.1007/s00190-020-01445-w, 2020.

Medley, B., McConnell, J. R., Neumann, T. A., Reijmer, C. H., Chellman, N., Sigl, M., and Kipfstuhl, S.: Temperature and Snowfall in Western Queen Maud Land Increasing Faster Than Climate Model Projections, Geophysical Research Letters, 45, 1472–1480, 10.1002/2017GL075992, 2018.

Mémin, A., Boy, J.-P., and Santamaría-Gómez, A.: Correcting GPS measurements for non-tidal loading, GPS Solutions, 24, 45, 10.1007/s10291-020-0959-3, 2020.

Menemenlis, D., Campin, J.-M., Heimbach, P., Hill, C., Lee, T., Nguyen, A., Schodlok, M., and Zhang, H.: ECCO2: High resolution global ocean and sea ice data synthesis, Mercator Ocean Quarterly Newsletter, 31, 13–21, 2008.

Niu, Y., Rebischung, P., Li, M., Wei, N., Shi, C., and Altamimi, Z.: Temporal spectrum of spatial correlations between GNSS station position time series, Journal of Geodesy, 97, 12, 10.1007/s00190-023-01703-7, 2023.

https://doi.org/10.5194/egusphere-2025-5358
Preprint. Discussion started: 7 November 2025

Niu, Y., Wei, N., Li, M., Rebischung, P., Shi, C., and Chen, G.: Quantifying discrepancies in the three-dimensional seasonal variations between IGS station positions and load models, Journal of Geodesy, 96, 31, 10.1007/s00190-022-01618-9, 2022.

Nordman, M., Virtanen, H., Nyberg, S., and Mäkinen, J.: Non-tidal loading by the Baltic Sea: Comparison of modelled deformation with GNSS time series, GeoResJ, 7, 14–21, 10.1016/j.grj.2015.03.002, 2015.

Pan, Y., Zhang, X., Jiao, J., Ding, H., and Shum, C. K.: Geodetic Evidence of the Interannual Fluctuations and Long-Term Trends Over the Antarctic Ice Sheet Mass Change, IEEE Journal of Selected Topics in Applied Earth Observations and Remote Sensing, 18, 4525–4535, 10.1109/JSTARS.2025.3528516, 2025.

Plag, H.-P., Rizos, C., Rothacher, M., and Neilan, R.: The Global Geodetic Observing System (GGOS): Detecting the Fingerprints of Global Change in Geodetic Quantities, Advances in Earth Observation of Global Change, 10.1007/978-90-481-9085-0_10, 2010.

Poropat, L., Kvas, A., Mayer-Gürr, T., and Dobslaw, H.: Mitigating temporal aliasing effects of high-frequency geophysical fluid dynamics in satellite gravimetry, Geophysical Journal International, 220, 257–266, 10.1093/gji/ggz439, 2019.

Reading, A. M., Stål, T., Halpin, J. A., Lösing, M., Ebbing, J., Shen, W., McCormack, F. S., Siddoway, C. S., and Hasterok, D.: Antarctic geothermal heat flow and its implications for tectonics and ice sheets, Nature Reviews Earth & Environment, 3, 814–831, 10.1038/s43017-022-00348-y, 2022.

Rebischung, P., Altamimi, Z., Métivier, L., Collilieux, X., Gobron, K., and Chanard, K.: Analysis of the IGS contribution to ITRF2020, Journal of Geodesy, 98, 49, 10.1007/s00190-024-01870-1, 2024.

Sandells, M. and Flocco, D.: Introduction to the Physics of the Cryosphere (Second Edition), Institute of Physics Publishing, Bristol, UNITED KINGDOM2022.

Santamaría-Gómez, A. and Mémin, A.: Geodetic secular velocity errors due to interannual surface loading deformation, Geophysical Journal International, 202, 763–767, 10.1093/gji/ggv190, 2015.

Scheinert, M., Engels, O., Schrama, E. J. O., Wal, W. v. d., and Horwath, M.: Geodetic observations for constraining mantle processes in Antarctica, Geological Society, London, Memoirs, 56, 295–313, doi:10.1144/M56-2021-22, 2023.

Shihora, L., Sulzbach, R., Dobslaw, H., and Thomas, M.: Self-attraction and loading feedback on ocean dynamics in both shallow water equations and primitive equations, Ocean Modelling, 169, 101914, 10.1016/j.ocemod.2021.101914, 2022a.

Shihora, L., Balidakis, K., Dill, R., Dahle, C., Ghobadi-Far, K., Bonin, J., and Dobslaw, H.: Non-Tidal Background Modeling for Satellite Gravimetry Based on Operational ECWMF and ERA5 Reanalysis Data: AOD1B RL07, Journal of Geophysical Research: Solid Earth, 127, e2022JB024360, 10.1029/2022JB024360, 2022b.

Springer, A., Karegar, M. A., Kusche, J., Keune, J., Kurtz, W., and Kollet, S.: Evidence of daily hydrological loading in GPS time series over Europe, Journal of Geodesy, 93, 2145–2153, 10.1007/s00190-019-01295-1, 2019.

Tankersley, M. D.: PolarToolkit: Python Tools for Convenient, Reproducible, and Open Polar Science, Journal of Open Source Software, 9, 6502, 10.21105/joss.06502, 2024.

van Dam, T., Collilieux, X., Wuite, J., Altamimi, Z., and Ray, J.: Nontidal ocean loading: amplitudes and potential effects in GPS height time series, Journal of Geodesy, 86, 1043–1057, 10.1007/s00190-012-0564-5, 2012.

https://doi.org/10.5194/egusphere-2025-5358
Preprint. Discussion started: 7 November 2025

van Dam, T. M. and Wahr, J.: Modeling environment loading effects: a review, Physics and Chemistry of the Earth, 23, 1077–1087, 10.1016/S0079-1946(98)00147-5, 1998.

van Dam, T. M., Blewitt, G., and Heflin, M. B.: Atmospheric pressure loading effects on Global Positioning System coordinate determinations, Journal of Geophysical Research: Solid Earth, 99, 23939–23950, 10.1029/94JB02122, 1994.

Williams, S. D. P. and Penna, N. T.: Non-tidal ocean loading effects on geodetic GPS heights, Geophysical Research Letters, 38, 10.1029/2011GL046940, 2011.

Williams, S. D. P., Bock, Y., Fang, P., Jamason, P., Nikolaidis, R. M., Prawirodirdjo, L., Miller, M., and Johnson, D. J.: Error analysis of continuous GPS position time series, Journal of Geophysical Research: Solid Earth, 109, 10.1029/2003JB002741, 2004.

Wu, S., Nie, G., Meng, X., Liu, J., He, Y., Xue, C., and Li, H.: Comparative Analysis of the Effect of the Loading Series from GFZ and EOST on Long-Term GPS Height Time Series, Remote Sensing, 12, 2822, 10.3390/rs12172822, 2020.